

Planck early results XIV: ERCSC validation and extreme radio sources

Planck Collaboration: P. A. R. Ade⁷⁵, N. Aghanim⁴⁹, E. Angelakis⁶⁸, M. Arnaud⁶², M. Ashdown^{60,4}, J. Aumont⁴⁹, C. Baccigalupi⁷³, A. Balbi²⁸, A. J. Banday^{79,8,67}, R. B. Barreiro⁵⁶, J. G. Bartlett^{3,58}, E. Battaner⁸¹, K. Benabed⁵⁰, A. Benoît⁴⁸, J.-P. Bernard^{79,8}, M. Bersanelli^{25,42}, R. Bhatia⁵, A. Bonaldi³⁸, L. Bonavera^{73,6}, J. R. Bond⁷, J. Borrill^{66,76}, F. R. Bouchet⁵⁰, M. Bucher³, C. Burigana⁴¹, P. Cabella²⁸, B. Cappellini⁴², J.-F. Cardoso^{63,3,50}, A. Catalano^{3,61}, L. Cayón¹⁸, A. Challinor^{53,60,10}, A. Chamballu⁴⁶, R.-R. Chary⁴⁷, X. Chen⁴⁷, L.-Y. Chiang⁵², P. R. Christensen^{71,29}, D. L. Clements⁴⁶, S. Colombi⁵⁰, F. Couchot⁶⁵, A. Coulais⁶¹, B. P. Crill^{58,72}, F. Cuttaia⁴¹, L. Danese⁷³, R. D. Davies⁵⁹, R. J. Davis⁵⁹, P. de Bernardis²⁴, G. de Gasperis²⁸, A. de Rosa⁴¹, G. de Zotti^{38,73}, J. Delabrouille³, J.-M. Delouis⁵⁰, F.-X. Désert⁴⁴, C. Dickinson⁵⁹, S. Donzelli^{42,54}, O. Doré^{58,9}, U. Dörl⁶⁷, M. Douspis⁴⁹, X. Dupac³², G. Efstathiou⁵³, T. A. Enßlin⁶⁷, F. Finelli⁴¹, O. Forni^{79,8}, M. Frailis⁴⁰, E. Franceschi⁴¹, L. Fuhrmann⁶⁸, S. Galeotta⁴⁰, K. Ganga^{3,47}, M. Giard^{79,8}, G. Giardino³³, Y. Giraud-Héraud³, J. González-Nuevo⁷³, K. M. Górski^{58,83}, S. Gratton^{60,53}, A. Gregorio²⁶, A. Gruppuso⁴¹, D. Harrison^{53,60}, S. Henrot-Versillé⁶⁵, D. Herranz⁵⁶, S. R. Hildebrandt^{9,64,55}, E. Hivon⁵⁰, M. Hobson⁴, W. A. Holmes⁵⁸, W. Hovest⁶⁷, R. J. Hoyland⁵⁵, K. M. Huffenberger⁸², M. Huynh⁴⁷, A. H. Jaffe⁴⁶, M. Juvela¹⁷, E. Keihänen¹⁷, R. Kesikitalo^{58,17}, T. S. Kisner⁶⁶, R. Kneissl^{31,5}, L. Knox²⁰, T. P. Krichbaum⁶⁸, H. Kurki-Suonio^{17,36}, G. Lagache⁴⁹, A. Lähteenmäki^{1,36}, J.-M. Lamarre⁶¹, A. Lasenby^{4,60}, R. J. Laureijs³³, N. Lavonen¹, C. R. Lawrence⁵⁸, S. Leach⁷³, J. P. Leahy⁵⁹, R. Leonardi^{32,33,21}, J. León-Tavares¹, M. Linden-Vørnle¹², M. López-Cañiego⁵⁶, P. M. Lubin²¹, J. F. Macías-Pérez⁶⁴, B. Maffei⁵⁹, D. Maino^{25,42}, N. Mandolesi⁴¹, R. Mann⁷⁴, M. Maris⁴⁰, F. Marleau¹⁴, E. Martínez-González⁵⁶, S. Masi²⁴, M. Massardi³⁸, S. Matarrese²³, F. Matthai⁶⁷, P. Mazzotta²⁸, P. R. Meinhold²¹, A. Melchiorri²⁴, L. Mendes³², A. Mennella^{25,40}, M. Mingaliev⁷⁷, M.-A. Miville-Deschênes^{49,7}, A. Moneti⁵⁰, L. Montier^{79,8}, G. Morgante⁴¹, D. Mortlock⁴⁶, D. Munshi^{75,53}, A. Murphy⁷⁰, P. Naselsky^{71,29}, P. Natoli^{27,2,41}, I. Nestoras⁶⁸, C. B. Netterfield¹⁴, E. Nieppola^{1,34}, H. U. Nørgaard-Nielsen¹², F. Noviello⁴⁹, D. Novikov⁴⁶, I. Novikov⁷¹, S. Osborne⁷⁸, F. Pajot⁴⁹, B. Partridge^{35*}, F. Pasian⁴⁰, G. Patanchon³, T. J. Pearson^{9,47}, O. Perdereau⁶⁵, L. Perotto⁶⁴, F. Perrotta⁷³, F. Piacentini²⁴, M. Piat³, E. Pierpaoli¹⁶, S. Plaszczynski⁶⁵, P. Platania⁵⁷, E. Pointecouteau^{79,8}, G. Polenta^{2,39}, N. Ponthieu⁴⁹, D. Poutanen^{36,17,1}, G. Prézeau^{9,58}, P. Procopio⁴¹, S. Prunet⁵⁰, J.-L. Puget⁴⁹, J. P. Rachen⁶⁷, W. T. Reach⁸⁰, R. Rebolo^{55,30}, M. Reinecke⁶⁷, C. Renault⁶⁴, S. Ricciardi⁴¹, T. Riller⁶⁷, D. Riquelme⁵¹, I. Ristorcelli^{79,8}, G. Rocha^{58,9}, C. Rosset³, M. Rowan-Robinson⁴⁶, J. A. Rubiño-Martín^{55,30}, B. Rusholme⁴⁷, A. Sajina³⁵, M. Sandri⁴¹, P. Savolainen¹, D. Scott¹⁵, M. D. Seiffert^{58,9}, A. Sievers⁵¹, G. F. Smoot^{19,66,3}, Y. Sotnikova⁷⁷, J.-L. Starck^{62,11}, F. Stivoli⁴³, V. Stolyarov⁴, R. Sudiwala⁷⁵, J.-F. Sygnet⁵⁰, J. Tammi¹, J. A. Tauber³³, L. Terenzi⁴¹, L. Toffolatti¹³, M. Tomasi^{25,42}, M. Tornikoski¹, J.-P. Torre⁴⁹, M. Tristram⁶⁵, J. Tuovinen⁶⁹, M. Türlér⁴⁵, M. Turunen¹, G. Umata³⁷, H. Ungerechts⁵¹, L. Valenziano⁴¹, J. Varis⁶⁹, P. Vielva⁵⁶, F. Villa⁴¹, N. Vittorio²⁸, L. A. Wade⁵⁸, B. D. Wandelt^{50,22}, A. Wilkinson⁵⁹, D. Yvon¹¹, A. Zacchei⁴⁰, J. A. Zensus⁶⁸, and A. Zonca²¹

(Affiliations can be found after the references)

Preprint online version: October 30, 2018

ABSTRACT

Planck's all-sky surveys at 30–857 GHz provide an unprecedented opportunity to follow the radio spectra of a large sample of extragalactic sources to frequencies 2–20 times higher than allowed by past, large-area, ground-based surveys. We combine the results of the *Planck* Early Release Compact Source Catalog (ERCSC) with quasi-simultaneous ground-based observations as well as archival data at frequencies below or overlapping *Planck* frequency bands, to validate the astrometry and photometry of the ERCSC radio sources and study the spectral features shown in this new frequency window opened by *Planck*. The ERCSC source positions and flux density scales are found to be consistent with the ground-based observations. We present and discuss the spectral energy distributions (SEDs) of a sample of “extreme” radio sources, to illustrate the richness of the ERCSC for the study of extragalactic radio sources. Variability is found to play a role in the unusual spectral features of some of these sources.

Key words. Surveys: radio sources—Radio continuum: galaxies—Radiation mechanisms: general

1. Introduction

This paper is one of a series based on observations of compact sources by the *Planck*¹ satellite that are included in the ERCSC (Planck Collaboration 2011c). Among these “Early

Results” *Planck* papers there are three that address the extragalactic radio source population. Planck Collaboration (2011d) examines statistical properties such as number counts and spectral index distributions, but only at frequencies ≥ 30 GHz. Planck Collaboration (2011e) incorporates *Planck* measurements and supporting ground-based and satellite observations to refine models for the physical properties of a sample of ~ 100 bright blazars. Here we address the observed diverse, sometimes peculiar, spectral properties of sources in the ERCSC, which include peaked-spectrum, flat-spectrum, upturn-spectrum and multicomponent-spectrum sources. We combine archival data as well as new, ground-based, radio observations with the *Planck*

* Corresponding author: B. Partridge, bpartrid@haverford.edu

¹ *Planck* (<http://www.esa.int/Planck>) is a project of the European Space Agency (ESA) with instruments provided by two scientific consortia funded by ESA member states (in particular the lead countries France and Italy), with contributions from NASA (USA) and telescope reflectors provided by a collaboration between ESA and a scientific consortium led and funded by Denmark.

data to construct SEDs from ~ 3 to ~ 200 GHz (the exact frequency coverage varies case by case), to validate the astrometry and photometry of radio sources in the ERCSC. The *Planck* data are also valuable for studying, for instance, high frequency peaked-spectrum sources that were previously underrepresented in radio source populations due to the lack of observations in the sub-millimeter regime. On the other hand, the ground-based data complement the *Planck* data, and are crucial in defining the spectral shape of some sources by extending the observed SEDs. We present a sample of sources with near-simultaneous *Planck* and ground-based observations (primarily employing the VLA, Effelsberg, IRAM and Metsähovi telescopes in the northern hemisphere, and ATCA in the southern hemisphere), to control for variability. We also investigate a small number of ERCSC sources at 30 to 70 GHz without clear identification in existing radio surveys.

1.1. The *Planck* mission

Planck (Tauber et al. 2010; Planck Collaboration 2011a) is the third generation space mission to measure the anisotropy of the cosmic microwave background (CMB). It observes the sky in nine frequency bands covering 30 to 857 GHz with high sensitivity and angular resolution from $32'$ to $5'$. The Low Frequency Instrument (LFI; Mandolesi et al. 2010; Bersanelli et al. 2010; Mennella et al. 2011) covers the 30, 44 and 70 GHz bands with amplifiers cooled to 20 K. The High Frequency Instrument (HFI; Lamarre et al. 2010; Planck HFI Core Team 2011a) covers the 100, 143, 217, 353, 545 and 857 GHz bands with bolometers cooled to 0.1 K. Polarisation is measured in all but the highest two bands (Leahy et al. 2010; Rosset et al. 2010). A combination of radiative cooling and three mechanical coolers produces the temperatures needed for the detectors and optics (Planck Collaboration 2011b). Two Data Processing Centers (DPCs) check and calibrate the data and make maps of the sky (Planck HFI Core Team 2011b; Zacchei et al. 2011). *Planck*'s sensitivity, angular resolution and frequency coverage make it a powerful instrument for Galactic and extragalactic astrophysics as well as cosmology.

The scan strategy employed in the *Planck* mission is described in Planck Collaboration (2011a). As the satellite spins, sources are swept over the focal plane, as indicated schematically in Figure 1. In the course of each day, the pointing axis of the telescope is adjusted by $\sim 1^\circ$, so a given source will follow a slightly different track across the focal plane; thus its flux density is the average of many such scans. In addition, since the data included in the ERCSC amount to ~ 1.6 full-sky surveys, some sources have been covered twice with a time separation of ~ 6 months. Finally, sources near the ecliptic poles, where the scan circles intersect, are often covered multiple times. It is thus important to keep in mind that the flux densities cited in this paper (and indeed in the ERCSC as a whole) are *averaged*. Figure 1 illustrates that flux measurements at 44 GHz are particularly susceptible to time-dependent effects, because of the wide spacing of the 44 GHz horns in the focal plane (see further discussion in § 5.2.2).

1.2. The ERCSC

The *Planck* Early Release Compact Source Catalog (Planck Collaboration 2011c) provides lists of positions and flux densities of compact sources at each of the nine *Planck* frequencies. For frequencies from 30 to 143 GHz (those mostly cited

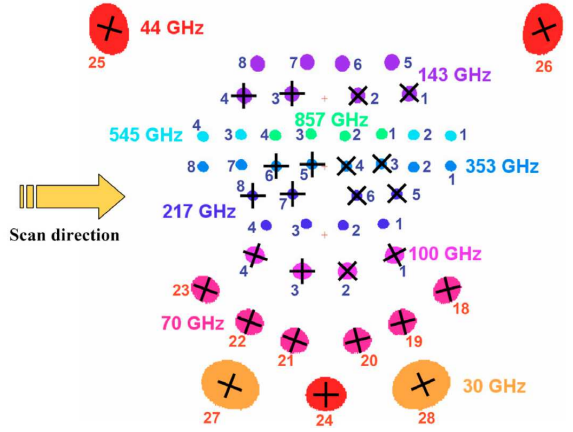


Fig. 1. Focal plane, showing spacing of the *Planck* receivers. Each day, the pointing is adjusted by $\sim 1^\circ$ in the vertical direction. Note that the wide separation of the three 44 GHz horns (two at the top, one at the bottom) causes the 44 GHz observations of a given source to take place at two times separated by 7–10 days for each scan.

in this paper), sources were detected using Powell Snakes techniques (Carvalho et al. 2009). In the four highest frequency channels, sources were located using the SExtractor method (Bertin & Arnouts 1996). A set of selection criteria was further applied to select sources that are included in the ERCSC. The primary criterion was a Monte Carlo assessment designed to ensure that $\geq 90\%$ of the sources in the catalogue are reliable and have a flux density accuracy better than 30%. External validation (also discussed in Planck Collaboration 2011c) shows that ERCSC met its reliability criterion, and we show evidence in § 4 that the flux density scale of ERCSC is accurate. Secondary selection criteria, including the elimination of extended sources, were also applied. Virtually all of the sources discussed in this paper, and the vast majority of extragalactic ERCSC sources, were unresolved by *Planck* and in many cases even at the much higher angular resolution of the VLA or other ground-based instruments.

The flux densities in the ERCSC are calculated using aperture photometry. The effective band centers or corresponding colour corrections depend to some degree on the spectrum of the source being observed. This relatively small dependence is discussed in the LFI and HFI instrument papers (Mennella et al. 2011; Planck HFI Core Team 2011a; Zacchei et al. 2011; Planck HFI Core Team 2011b). We adopt here (and list in Table 1) the effective central frequencies defined in those papers, and the colour corrections defined for a source with a spectral index $\alpha = -0.5$ (using the convention $S_\nu \propto \nu^\alpha$). To obtain the correct flux density for an assumed narrow band measurement, we divide the tabulated ERCSC flux densities by the colour correction factor at the corresponding central frequency. After the release of the ERCSC, it was found that the correction for aberration introduced by the motion of the satellite had not been correctly made. This introduces small ($< 0.35'$) errors in the catalogued positions of sources; these can in turn produce very small errors ($< 1\%$) in flux densities. We have not corrected the ERCSC flux densities for this small effect.

In the next section, we describe briefly some general properties of the extragalactic radio sources in the ERCSC. We describe in § 3 related ground-based observations. In § 4, we discuss the identification of sources, positional accuracy and flux density scales, comparing those obtained from *Planck* with ground-based measurements. This parallels the validation work

Table 1. Parameters of *Planck* bands employed in this paper.

Planck Band	Central Frequency [GHz]	Colour Correction	Beam FWHM [arcmin]
30	28.5	1.037	32.6
44	44.1	1.018	27.0
70	70.3	1.031	13.0
100	100	0.999	9.94
143	143	1.006	7.04
217	217	0.993	4.66
353	353	0.990	4.41

discussed in [Planck Collaboration \(2011c\)](#). Variability of source luminosity and the issue of different resolutions are also discussed. We present and discuss in § 5 several examples of interesting classes of extragalactic radio sources. We conclude in the final section and point towards further research on these radio sources and many others contained in the ERCSC.

2. Radio sources in the ERCSC

The ERCSC contains hundreds of extragalactic radio sources at frequencies up to 143 GHz. At frequencies > 100 GHz, the *Planck* surveys are unique. At 30 and 70 GHz, the higher sensitivity and resolution offered by *Planck* allow us to detect more sources in a single sky survey than in seven years of survey by the WMAP satellite ([Gold et al. 2011](#)).

A major finding from the analysis of ERCSC is that many bright radio sources have relatively flat ($\alpha > -0.5$) radio spectra extending up to and sometimes beyond 143 GHz. The vast majority of the extragalactic sources detected at 100, 143 and 217 GHz are synchrotron-dominated radio sources and not dusty galaxies. The statistical properties of radio sources in the ERCSC are discussed in much greater detail in the companion paper, [Planck Collaboration \(2011d\)](#).

A second finding is the absence of compelling evidence for any new class of extragalactic radio sources. At 30 to 70 GHz, more than 90 % of the extragalactic sources were reliably associated with radio sources in other large area surveys conducted at 8–20 GHz ([Planck Collaboration 2011c](#)). Still others have plausible identifications in lower frequency radio catalogues. We discuss those ERCSC sources without clear identification in § 5.4 since they may potentially contain new types of sources.

Many of the identified radio sources are blazars, some of them clearly variable (see a detailed discussion in [Planck Collaboration 2011e](#)). In § 5, we discuss a small number of extreme or unusual radio sources as additional examples of the scientific richness the ERCSC provides for the study of extragalactic radio sources.

The *Planck* data used here are drawn entirely from the ERCSC. These data are supplemented by ground-based observations at frequencies below and overlapping the *Planck* frequency bands, which were generally made quasi-simultaneously with the *Planck* observations of a given source (within 7–10 days, typically). This step was taken to monitor and control for variability.

3. Ground-based observations

In planning the *Planck* mission, it was recognised that the science yield of *Planck*'s millimeter and FIR sky surveys would be increased if accompanying ground-based observations could be

made. These include, but are not limited to, radio observations at frequencies below and overlapping *Planck* frequency bands, optical observations for source identification and both ground- and satellite-based X- and γ -ray observations. This paper discusses only the supporting radio observations; for a discussion of the approximately simultaneous X- and γ -ray observations, see [Planck Collaboration \(2011e\)](#). Table 2 provides information on the radio observatories that are involved and produced data used in this paper. Most of the radio observations were made *preemptively*—that is, we observed sources expected to be detected by *Planck* at about the same time they passed through the *Planck* beam. The POFF software ([Massardi & Burigana 2010](#)) was used to predict which sources would be seen by *Planck* in a given week. Obviously, only previously known sources can be observed preemptively. We later conducted a small number of follow-up observations on ERCSC sources.

In the southern hemisphere, a substantial amount of time was obtained at the Australia Telescope Compact Array (ATCA) to make preemptive observations at a wide range of frequencies up to and overlapping with the *Planck*. The Planck-ATCA Co-eval Observations (PACO) project ([Massardi et al. 2011](#)) consists of several-epoch observations of a compilation of sources selected from the Australia Telescope 20 GHz survey (AT20G, [Murphy et al. 2010](#)) with $|b| > 5^\circ$. Observations were made with ATCA in the frequency range between 4.5 and 40 GHz at epochs close in time to the *Planck* observations over the interval from July 2009 to August 2010. The PACO sample includes a complete flux density limited and spectrally selected sample over the whole Southern sky; 147 PACO point-like sources have at least one observation within 10 days of the *Planck* observations.

In the northern hemisphere, quasi-simultaneous cm/mm radio spectra for a large number of *Planck* blazars have been obtained within the framework of a *Fermi*-GST related monitoring program of γ -ray blazars (F-GAMMA program, [Fuhrmann et al. 2007](#); [Angelakis et al. 2008](#)). The frequency range spans from 2.64 GHz to 142 GHz using the Effelsberg 100 m and IRAM 30 m telescopes. The Effelsberg measurements were conducted with the secondary focus heterodyne receivers at 2.64, 4.85, 8.35, 10.45, 14.60, 23.05, 32.00 and 43.00 GHz. The observations were performed quasi-simultaneously with cross-scans, that is slewing over the source position in azimuth and elevation direction with the number of sub-scans adjusted to reach the desired sensitivity (for details, see [Fuhrmann et al. 2008](#); [Angelakis et al. 2008](#)). Subsequently, pointing off-set correction, gain correction, atmospheric opacity correction and sensitivity correction were applied to the data. The IRAM 30 m observations were carried out with calibrated cross-scans using the EMIR horizontal and vertical polarisation receivers operating at 86.2 and 142.3 GHz. The opacity corrected intensities were converted into the standard temperature scale and finally corrected for small remaining pointing offsets and systematic gain-elevation effects. The conversion to the standard flux density scale was done using the instantaneous conversion factors derived from frequently observed primary (Mars, Uranus) and secondary (W3(OH), K3-50A, NGC7027) calibrators.

In the northern hemisphere, some data also come from the Metsähovi telescope operating at 37 GHz. The observations were made with the 13.7 m Metsähovi radio telescope, which is a radome-enclosed, paraboloid antenna situated in Finland. The measurements were made with a 1 GHz-band dual-beam receiver centered at 36.8 GHz. The observations are ON–ON, alternating the source and the sky in each feed horn. A typical integration time to obtain one flux density data point is 1200–1400 s. The detection limit of the telescope at 37 GHz is of the order of

Table 2. Ground-based radio observations.

Observatory	Project Leaders	Frequencies [GHz]
ATCA, Australia	Massardi	4.5–40
Effelsberg, Germany	Fuhrmann, Angelakis and Rachen	2.6–43
IRAM, Spain	Fuhrmann, Ungerechts and Rachen	86.2, 142.3
Metsähovi, Finland	Lähteenmäki and Tornikoski	37
VLA/EVLA, USA	Partridge and Sajina	5, 8, 22, 43

0.2 Jy under optimal conditions. Data points with a signal-to-noise ratio < 4 are treated as non-detections. The flux density scale is set by observations of DR21. Sources NGC7027, 3C274 and 3C84 are used as secondary calibrators. A detailed description of the data reduction and analysis is given in (Teraesranta et al. 1998). The error estimate in the flux density includes the contribution from the measurement rms and the uncertainty of the absolute calibration.

In addition, small amounts of time, scattered throughout the first 17 months of the *Planck* mission, were obtained at the Very Large Array (VLA) of the National Radio Astronomy Observatory (NRAO). Observations at the VLA began 24 July 2009, slightly before the beginning of *Planck*'s first sky survey. The first set of observations on 24 July 2009 is the only set not approximately simultaneous with *Planck* observations. VLA/EVLA measurements continued at irregular intervals until November 2010, with a substantial gap in the spring of 2010 when the VLA was converted to the EVLA. Most of the VLA and EVLA runs were brief 1–2 hour chunks of time; 5–8 *Planck* sources were typically observed per hour, besides flux calibrators and phase calibrators. In many cases, VLA flux and phase calibrators were of interest themselves because they were bright enough to be detected by *Planck*. The integration times were typically 30 seconds at 4.86 GHz and 8.46 GHz, 100 seconds at 22.46 GHz, and 120 seconds at 43.34 GHz. All u-v data were flagged, calibrated and imaged using standard NRAO software: AIPS or CASA. The flux density measurements were calibrated against one or both of the primary calibrators used by NRAO: 3C48 or 3C286.

The positions and flux densities of sources observed by the VLA are listed in Table 3. Since the VLA flux densities are accurate to a few percent for these bright sources, individual uncertainties are not included. Typical 1σ errors at 22 GHz ranged from 2 mJy (for the fainter sources) to 15 mJy (for brighter sources); and from 3–15 mJy at 43 GHz; both are small compared to the uncertainties in Planck flux densities. The VLA (EVLA) was in different configurations at different times; hence the angular resolution of the array was changing. Additionally, for a given configuration, the resolution was much finer at higher frequencies. We thus flagged sources that showed signs of resolution in any configuration at any frequency. In general, the VLA observations were timed to occur during the same week as *Planck* was expected to see a given source, but that was not always possible. Therefore, each observation is tagged with a date in Table 3, to be compared with the dates of observation tabulated in the ERCSC. Given that the typical timescale for variability of radio sources is roughly weeks to months (see

e.g., Hovatta et al. 2008; Nieppola et al. 2009), we were able to control for variability to some degree. Nevertheless, it must be borne in mind that the ground-based observations were not always taken at the same time *Planck* was observing a source. The *Planck* beams at different frequencies also swept over a source at different times due to the extended layout of its focal plane. We use this set of data in § 4 to check the positional and photometric accuracy of ERCSC sources.

4. Identification and validation

To construct SEDs that include measurements from both *Planck* and ground-based telescopes, we need to ensure that the identification of a source in the ERCSC has been correctly made, and that the flux density scales are consistent. Both properties were extensively checked as part of the validation work of the ERCSC (Planck Collaboration 2011c). We present here the comparison of quasi-simultaneous VLA and *Planck* observations of a set of bright radio sources.

4.1. Source identification

Identifying a source for supporting ground-based observations requires an understanding of the astrometric accuracy of the ERCSC. In Figure 2, we show a comparison of ERCSC source positions at 30 and 70 GHz with those measured for the presumed identification by the VLA at 22 GHz. The VLA positions for such bright sources are typically accurate to a few arcseconds even for the most compact configurations. Figure 2 indicates that (a) the ERCSC meets its specification of having a positional accuracy good to FWHM/5 (or $\sim 6.5'$ at 30 GHz); (b) a search radius of 1/2 FWHM of the beam around each ERCSC source position is sufficient to locate any related source; and (c) any bright radio source within a few arcmin of the ERCSC position is likely the correct low frequency counterpart. This last point can be made more quantitative using the AT20G survey, which covers the entire southern hemisphere to ~ 40 mJy at 20 GHz, and is essentially complete above 100 mJy. The density of sources with $S > 100$ mJy is ~ 0.25 per square degree, and the integral counts of sources have a slope of -1.15 . Thus we expect on average 0.07 sources-deg $^{-2}$ above 300 mJy, the threshold we applied when cross-correlating AT20G sources with the ERCSC. At 30 GHz, the probability of a random AT20G source appearing within 16.25' of a given ERCSC source is $\sim 1.6\%$. The ERCSC contains several hundred extragalactic sources, depending on frequency; only 5–8 of these might be falsely identified or confused. Additionally, all the sources described in § 5 fall within a radius of 5' of the ERCSC position, further reducing the chance coincidence rate by a factor of ~ 10 . The ERCSC source positions were also independently compared to those recorded for several hundred bright quasars. The median scatters in offset are 2.0', 1.7', 1.1', 0.8', 0.7' and 0.3' for the *Planck* frequency bands 30 to 217 GHz (Planck Collaboration 2011c). This is consistent with our observations shown in Figure 2.

4.2. Comparison of flux density scales

The flux density scale of *Planck* is ultimately tied to the amplitude of the CMB dipole, and careful measurements of the angular resolution of *Planck* and the ground-based instruments are required in order to convert from temperature units to flux density (Planck Collaboration 2011c). Since the calibration standard was the very large angular scale dipole signal, it is important to

Table 3. VLA observations on a set of bright ERCSC sources.

ERCSC name	VLA RA [J2000]	VLA Dec [J2000]	$S_{4.86\text{ GHz}}$ [Jy]	$S_{8.46\text{ GHz}}$ [Jy]	$S_{22.46\text{ GHz}}$ [Jy]	$S_{43.34\text{ GHz}}$ [Jy]	VLA obs. date [yymmdd]	<i>Planck</i> obs. date ^d [yymmdd]
G052.38-36.49	21:34:10.3	-01:53:17	1.698	1.218	091103	091102, 091103, 091108–091110, 100509–100511, 100517
G056.70+80.65 ^b	13:31:08.3	30:30:33	7.485	5.202	2.516	1.444	091022, 100103	091230, 091231
G075.68-29.62	22:03:26.9	17:25:48	0.987	1.055	1.035	1.073	091211	091121, 091128–091202, 100524–100527, 100602, 100603
G077.45-38.54	22:32:36.4	11:43:51	5.594	5.827	4.407	3.606	091211	091127, 091203–091207, 100531–100603 100506–100510, 100519, 100520
G085.72+26.08	18:24:07.1	56:51:01	1.403	1.876	1.771	1.258	090724	090827–090829, 100417–100422, 100503, 100504
G085.86+83.31	13:10:28.7	32:20:44	1.427	2.133	2.856	1.977	100103	091221–091225, 100102, 100103
G085.95-18.77 ^c	22:03:15.0	31:45:38	2.165	2.495	2.576	2.841	091211	091202, 091203, 091211–091215, 100531–100603
G086.12-38.18 ^c	22:53:57.8	16:08:54	9.463	8.176	11.834	21.570	091211	091206, 091207, 091213–091216
G090.11–25.64	22:36:22.5	28:28:57	1.285	1.273	1.412	1.547	091211	091210, 091211, 091218–091221
G090.14+09.66	20:23:55.8	54:27:36	0.952	1.132	0.804	0.502	090724	091222, 091223, 100517, 100518
G092.62–10.44	22:02:43.3	42:16:39	3.994	3.996	3.440	3.085	091211	091213, 091214, 091222–091226, 100606, 100607
G096.08+13.77	20:22:06.7	61:36:59	3.110	3.800	1.946	0.836	090724	091220–091222, 100103–100108, 100526–100531, 100602
G097.46+25.04	18:49:16.1	67:05:42	1.284	2.431	3.553	2.956	090724	091012–091014, 091017–091022, 091112–091114, 091225–091227, 100112–100119, 100512–100514, 100516–100521
G098.28+58.29	14:19:46.6	54:23:14	1.178	1.249	1.231	1.176	100103	091206, 091207, 091209–091212, 091226, 091227
G098.51+25.79	18:42:33.6	68:09:25	0.765	0.892	0.676	0.461	090724	091013–091015, 091110–091112, 091231, 100101, 100116–100119, 100121, 100122, 100514–100516, 100518–100521, 100523, 100524
G110.05+29.07	18:00:45.7	78:28:04	2.098	2.850	2.598	1.936	090724	091011–091016, 091026, 091027, 100202, 100203, 100214–100219
G126.44–64.29 ^c	00:57:34.9	-01:23:28	0.338	0.097	0.060	0.070	091103	100107, 100108
G128.95+11.97	02:17:30.8	73:49:33	4.168	4.090	2.623	1.709	090827	090911–090914, 090920, 090921, 100211, 100212, 100217–100220
G133.94–28.63 ^b	01:37:41.3	33:09:35	5.426	3.140	1.098	0.501	090827, 091211	100130, 100131
G143.55+34.41	08:41:24.4	70:53:42	1.762	1.485	2.267	2.900	091022	091012–091014, 091019, 100316, 100317, 100324–100327
G145.58+64.96	11:53:24.5	49:31:09	1.167	0.949	0.885	0.798	100103	091116–091119, 091125, 091126, 100511, 100512, 100522–100526
G174.47+69.79	11:30:53.3	38:15:19	1.334	1.356	1.019	0.680	100103	091121, 100527
G195.26–33.13	04:23:15.8	-01:20:33	7.500	7.289	091103	090828–090830, 090903, 100221, 100225–100227
G199.42+78.39	11:59:31.8	29:14:44	1.609	1.530	1.416	1.141	100103	091204–091207, 091214, 100531, 100601
G200.06+31.89	08:30:52.1	24:11:00	1.269	1.246	1.050	0.825	091022	091021–091023, 091027, 100409, 100410, 100414–100416
G208.18+18.75	07:50:52.0	12:31:05	3.685	4.486	4.400	3.939	091022	091014–091016, 091020, 100404, 100408–100410
G211.33+19.05	07:57:06.6	09:56:35	1.143	1.530	1.863	1.846	091022	091015–091018, 091022, 100406, 100410–100412
G216.97+11.36	07:39:18.0	01:37:04	1.143	1.260	1.514	1.553	091022	091012–091014, 100408–100410
G221.26+22.36	08:25:50.3	03:09:24	0.777	0.737	0.668	0.648	091022	091024, 091025, 100419, 100420
G251.59+52.70	10:58:29.6	01:33:59	3.193	4.186	5.317	5.078	100103	091207–091210, 091216, 100524, 100530–100602
G255.00+81.65	12:24:54.5	21:22:47	1.233	1.267	1.412	1.184	100103	091218–091221
G283.75+74.54 ^c	12:30:49.4	12:23:28	62.000	39.000	12.000	...	100103	091226–091229, 100104, 100628, 100629

Notes. ^(a) *Planck* observation dates record the days that the source is observed by any of the 30, 44 and 70 GHz channels. ^(b) Standard VLA flux calibrator, observed twice. Reported flux densities are the average of the two observations. ^(c) Resolved source in the VLA.

confirm that flux density measurements of compact, unresolved, sources are accurate.

A potential complication in comparing flux densities is the greatly different angular resolution of *Planck* and the ground-based instruments. As discussed above, depending on the frequency and configuration, the angular resolution of the VLA can be as small as a fraction of an arcsecond, whereas the *Planck* beams are typically many arcminutes in size. Thus the VLA can “miss” flux included in the *Planck* beam. To first order, we take account of this by excluding from the flux density comparison any source seen to be resolved at any frequency by the

VLA (see Table 3). A clear example of such a source is 3C274 (J1230+1223).

We then compare in Figure 3 the VLA measurements with the ERCSC flux densities at 30, 44 and 70 GHz. The VLA 22 and 43 GHz measurements were used to interpolate the VLA flux densities to the center frequency of *Planck* 30 GHz band. In the case of 44 GHz, the VLA measurements centered at 43.34 GHz and the *Planck* measurements centered at 44.1 GHz were directly compared without any correction. We performed least squares fits to the data in the linear regime. The agreement at 30 GHz (28.5 GHz to be precise) is very good, with the mea-

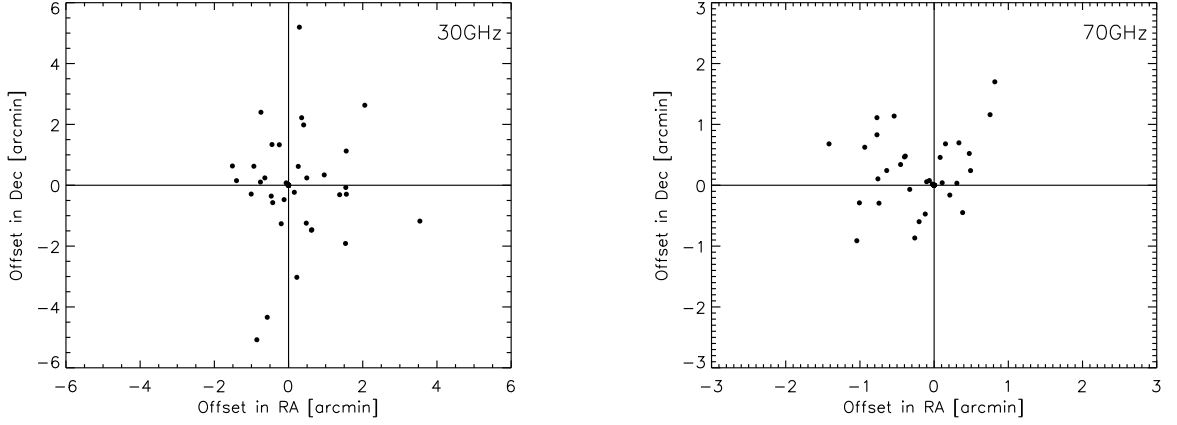


Fig. 2. Comparison of the VLA measurements made at ~ 22 GHz with the ERCSC source positions at 30 GHz (left) and 70 GHz (right).

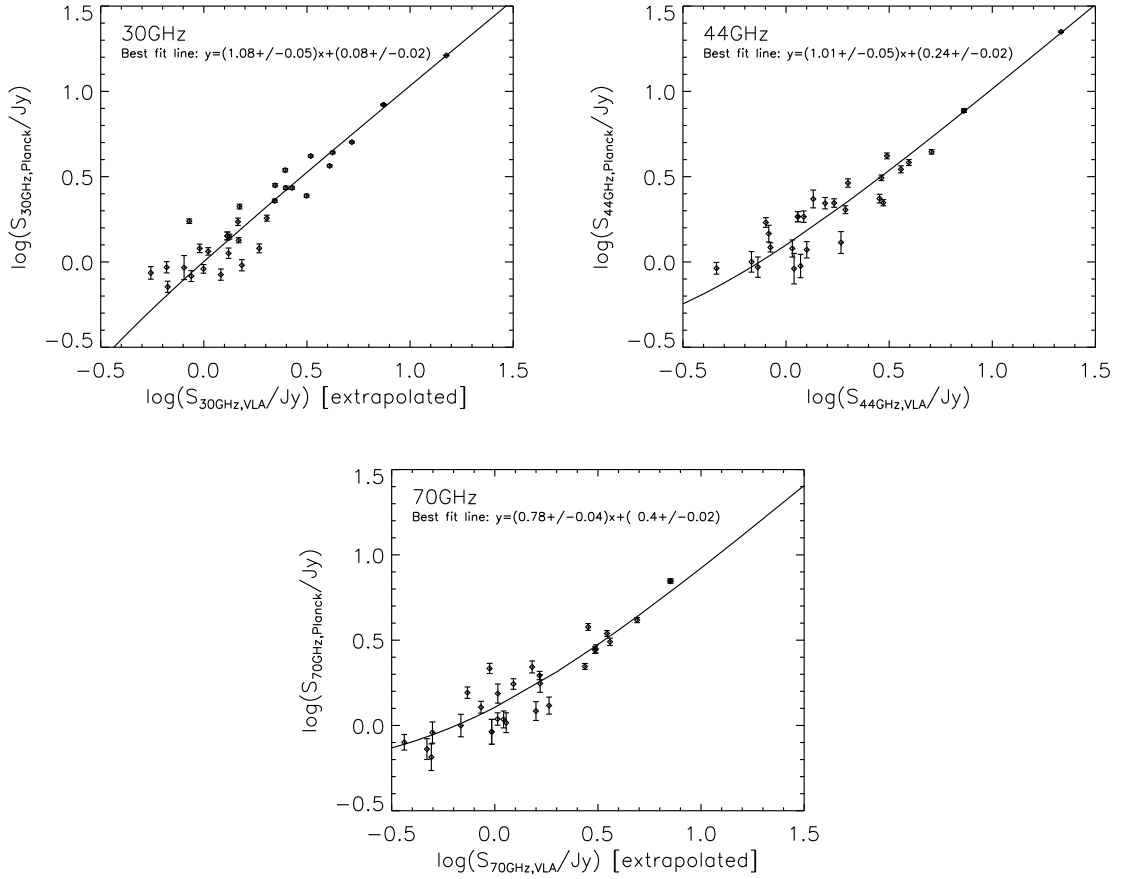


Fig. 3. *Upper left:* Comparison of *Planck* measurements in the “30 GHz” band with interpolated values from the VLA. *Upper right:* *Planck* vs. VLA measurements at 44 GHz. *Lower center:* *Planck* measurements at 70 GHz compared to the *extrapolated* VLA measurements. Note that although the log-log plot is presented for clarity, the fits were done on the *linear* data.

sured slope equal to 1.08 and an intercept of 0.08. At 44 GHz, the agreement is also reasonably good, with a measured slope of 1.01 and an intercept of 0.24.

At 70 GHz, we *extrapolate* the VLA measurements from 43 GHz using the 22–43 GHz spectral index. As shown in Figure 3, the extrapolated VLA values differ from the *Planck* values by $\sim 20\%$. There is strong evidence, presented in the companion

paper (Planck Collaboration 2011d), that the spectral index of radio sources detected by *Planck* steepens at frequencies above 70 GHz or perhaps 44 GHz for some sources. Thus some of our extrapolated VLA 70 GHz measurements may be biased high. Green Bank Telescope (GBT) 90 GHz measurements of a sample of VLA sources (Sajina et al. 2011), show that spectral curvature indeed plays a role. Among our VLA sample, 2 sources

have 90 GHz measurements. Replacing the extrapolated 70 GHz values with interpolated ones from VLA 44 GHz and GBT 90 GHz changes the slope of the best fit line to be closer to unity, from 0.78 to 0.86. We emphasise that the 90GHz observations were not made simultaneously with the *Planck* measurements, so they are less well controlled for variability than the quasi-simultaneous VLA (or EVLA) observations.

We also examined the median ratios of the *Planck* measurements and the extrapolated VLA flux densities. These are respectively 1.08 ± 0.04 , 1.12 ± 0.07 and 0.99 ± 0.06 for the 30, 44 and 70 GHz bands. These median values have the advantage over the linear fits in that they effectively force a zero intercept and mitigate the effect of outliers. The median ratios confirm the good agreement at 30 and 44 GHz and show that the agreement between our VLA and *Planck* flux densities at 70 GHz is better than implied by the linear fit. There is still, however, substantial scatter with the standard deviations of these ratios being 0.22, 0.38 and 0.29 for the 30, 44 and 70 GHz bands, respectively. The scatter is likely dominated by the intrinsic variability of our sources.

5. Extreme radio sources

In this section, we present several examples of sources illustrating the broad range of high frequency spectral behavior in bright, extragalactic radio sources as observed by *Planck*. This is not intended as an exhaustive list of extreme sources or an extensive discussion to explore the phenomenology of these sources, but rather a sample from the rich data set provided in the ERCSC. Here we employ both *Planck* and ground-based observations, using the latter to extend the source SEDs to lower frequencies. In some cases, the ground-based observations were made at roughly the same time as *Planck* observed the source, as mentioned in § 3. Archival data were used when such nearly simultaneous observations were not available.

5.1. Peaked spectrum sources

The term Gigahertz-Peaked-Spectrum (GPS) sources, in principle, refers to a morphological type of the radio spectra, namely, to a spectral index $\alpha > 0$ for $\nu < \nu_p$, and $\alpha < 0$ for $\nu > \nu_p$ with a peak frequency ν_p in the GHz regime. The GPS phenomenon was originally thought to be associated with compact, putatively very young radio sources (O’Dea 1998), and in fact many examples for this association have been found (Conway 2002). Recent research, however, has shown that a large fraction of sources with GPS features are not of this type, but associated with compact, beamed jet sources, commonly identified as blazars. These two classes produce slightly different spectra: the former shows a narrow peak, while the latter is typically broadly peaked. To date, however, the only secure method to distinguish between them is to employ VLBI observations, revealing the source morphology (Bolton et al. 2006; Vollmer et al. 2008). In this paper, we use the term “GPS sources” purely phenomenologically, and discuss in the following sections the different, known, classes of sources for which we have examples in the ERCSC and also a set of ERCSC sources that are candidate GPS sources.

5.1.1. ERCSC spectra of known Compact Symmetric Objects

One class of GPS sources is Compact Symmetric Objects (CSO), thought to be either very young or very recently activated radio

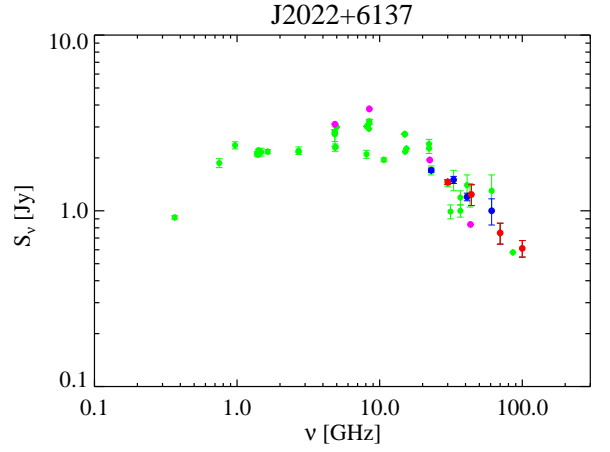


Fig. 4. SED of a known CSO source, J2022+6137. *Planck* measurements are shown in red, *WMAP*-7yr flux densities in blue, our new VLA measurements in pink and archival data obtained from NED in green.

galaxies (Owsianik & Conway 1998). Mapped with VLBI resolution, these sources show a typical, symmetric radio-double morphology, but with linear extensions of 10 pc or less. They produce GPS type spectra by essentially single-zone synchrotron emission with synchrotron self-absorption causing a spectral turn-over at $\nu > 1$ GHz (O’Dea 1998). Unlike blazars, their emission is most likely not Doppler boosted, and they show no hint of fast variability, although their interpretation as young radio galaxies suggests that a spectral evolution over time scales of decades may be possible. There is also a well-established connection between the peak frequency of a CSO-type GPS source and its linear extent: $d \sim 100\nu_p^{-1}$ pc, with ν_p in GHz. Thus sources with peak frequencies in the *Planck* regime would point to objects at most a few parsecs in linear size. Previously, populations of sources peaking above an observed frequency of 10 GHz (in the observer’s frame) might have been strongly under-represented because they are relatively faint at the low frequencies where most large surveys have been made. *Planck* opens the possibility of detecting such “extreme GPS” sources, or “high frequency peakers” in the nomenclature of Dallacasa et al. (2000). In addition, *Planck* allows the examination of the spectral decline of GPS sources at frequencies far above the peak frequency where optically thin synchrotron radiation is thought to dominate the emission. In Figure 4, we show the spectrum of one known CSO source, J2022+6137 (B2021+614 from Conway 2002). *Planck* data have been combined with archival data as CSO sources are not expected to be variable.

5.1.2. Additional high frequency peakers in ERCSC

As mentioned above, *Planck* observations make possible the detection and confirmation of rare, bright, GPS sources with very high peak frequencies. We provide in Table 4 a list of potential GPS sources that show convex SEDs constructed using the 30 to 143 GHz ERCSC data, along with the archival data at 20, 8.6 and 4.8 GHz (Murphy et al. 2010; Healey et al. 2007) if available. We restricted our search to $|b| > 10^\circ$ sources. While all of the tabulated sources display spectral peaks in the *Planck* frequency range, there is no guarantee that they are particularly young and compact CSO sources. Indeed, some of these bright sources have been previously studied, and most of them appear

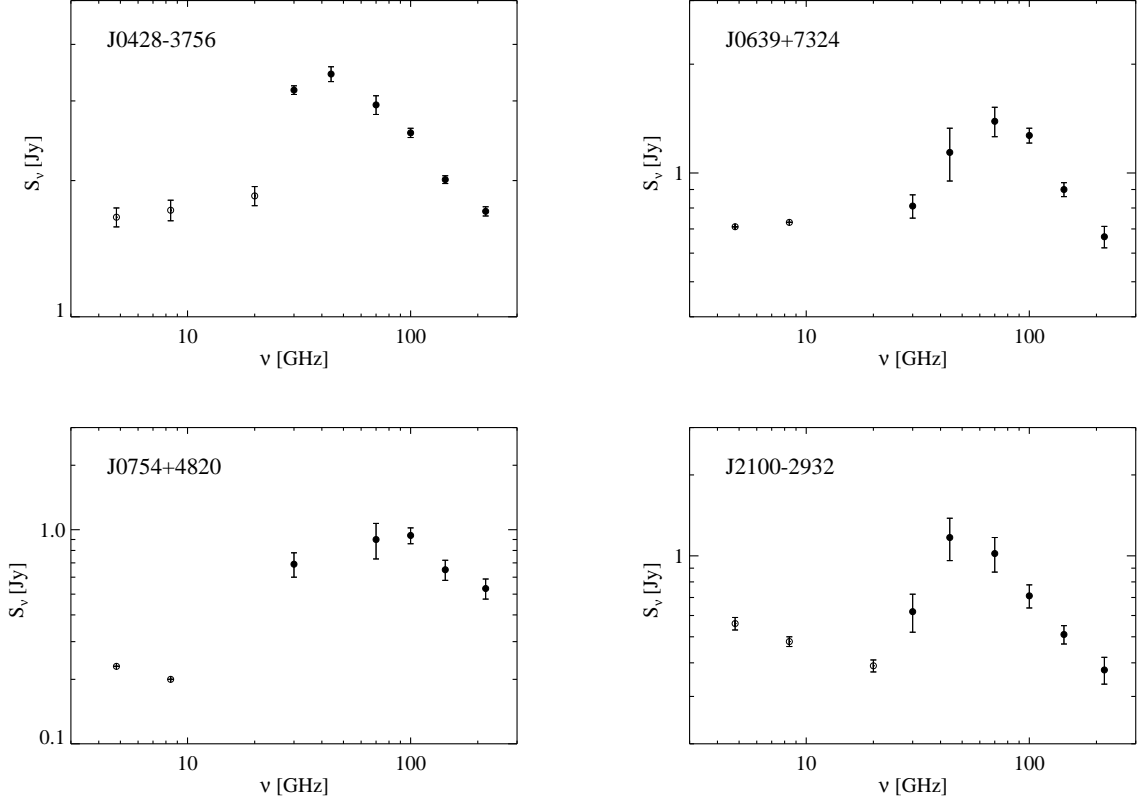


Fig. 5. SEDs of sources that show spectral peak in the *Planck* bands. ERCSC data are shown in filled circles and low frequency archival data are shown in open circles.

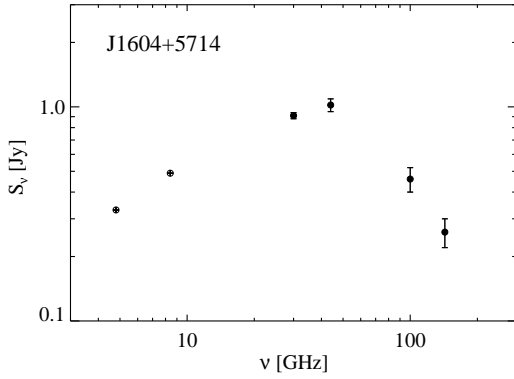


Fig. 6. With the additional *Planck* data, source J1604+5714 is a newly disclosed GPS source candidate that previously showed an inverted spectrum at low frequencies. ERCSC data are shown in filled circles and low frequency archival data are shown in open circles.

to be variable flat spectrum sources (see the notes in Table 4 and Tornaiainen et al. 2005). We discuss sources of this kind in more detail in § 5.2.

Figure 5 shows four sources that are quite undistinguished in low frequency catalogues, but reveal peaks in the *Planck* frequency range. Note that sources J0639+7324, J0754+4820 and J2100–2932 all present peaks at 70 GHz or higher. The recorded redshift of J0639+7324 is 1.85; thus the rest frame frequency of the emission peak is extremely high at ~200 GHz. In addition,

Planck data also helped to disclose the GPS-like spectrum for some sources that show inverted spectra at lower frequencies, as in the case of J1604+5714 (Figure 6).

As already mentioned, it is not possible from spectral information alone to identify high frequency peakers in the ERCSC with a new, very compact, radio source population. In fact, all but 5 sources in Table 4 can be identified with known blazars in the Roma-BZCAT blazar catalogue (Massaro et al. 2008). Out of the five exceptions, 3 are further associated with blazars in the CGRaBS blazar catalogue (Healey et al. 2008). The last two sources are identified as NGC1218 (J0308+0405) and HB89 2002–185 (J2005–1821) in NED. The SEDs of these two sources are shown in Figure 7. NGC1218 has a typical steep spectrum of radio galaxy up to 20 GHz, then a bump is seen at ~40 GHz. Since WMAP (in the 7 year co-added map) did not catch this feature whereas *Planck* did (during its 1.6 sky surveys), this peak is clearly caused by variability, suggesting some blazar like features in the galaxy, likely from close to the center. The spectral feature of HB89 2002-185 is evidently similar to that of source J2100–2932 in Figure 5 which has been identified as a flaring blazar. Therefore we suggest that this source could very well be a blazar. Further observations are needed to confirm this assumption. Our finding that the peaked spectra in many bright sources is the result of flaring is consistent with earlier discussions by Tornikoski et al. (2001); Tornaiainen et al. (2005); Bolton et al. (2006).

Table 4. GPS source candidates in the ERCSC.

Name	RA	Dec	$S_{143\text{ GHz}}$ [Jy]	$S_{100\text{ GHz}}$ [Jy]	$S_{70\text{ GHz}}$ [Jy]	$S_{44\text{ GHz}}$ [Jy]	$S_{30\text{ GHz}}$ [Jy]	$S_{20\text{ GHz}}$ [Jy]	$S_{8.6\text{ GHz}}$ [Jy]	$S_{4.8\text{ GHz}}$ [Jy]	Redshift	Notes
J0010+1058	00:10:35.5	10:58:34	1.40±0.05	1.85±0.09	2.15±0.20	2.77±0.18	2.44±0.08	...	0.25	0.44	0.089338	B
J0051-0651	00:51:14.9	-06:51:00	1.07±0.05	1.30±0.09	1.55±0.20	1.59±0.21	1.30±0.09	1.28±0.06	0.76	0.84	1.975000	B
J0118-2140	01:18:54.2	-21:40:55	0.76±0.04	0.86±0.07	1.34±0.16	...	1.16±0.07	0.88±0.06	0.91±0.05	0.88±0.04	1.161000	B
J0121+1149	01:21:45.6	11:49:37	0.82±0.07	1.09±0.10	0.99±0.21	1.84±0.24	1.92±0.09	...	1.87	1.13	0.570000	B
J0137-2430	01:37:41.8	-24:30:07	1.81±0.06	2.13±0.08	2.89±0.17	2.54±0.16	2.49±0.08	1.21±0.08	1.41±0.07	1.56±0.08	0.837000	B
J0253-5441	02:53:32.6	-54:41:17	1.32±0.05	1.78±0.07	1.69±0.15	2.68±0.15	2.38±0.07	1.93±0.10	1.65±0.08	1.43±0.07	0.539000	B, V
J0308+0405	03:08:22.8	04:05:53	0.61±0.06	0.90±0.09	1.32±0.17	1.45±0.17	1.17±0.07	0.028653	
J0334-4008	03:34:20.6	-40:08:53	1.41±0.04	1.72±0.06	1.89±0.13	2.36±0.11	2.35±0.06	1.27±0.06	1.12±0.06	0.94±0.05	1.445000	B, V
J0423-0120	04:23:16.3	-01:20:31	5.27±0.07	6.51±0.08	7.24±0.19	7.85±0.17	8.65±0.09	6.00±0.29	2.41	4.36	0.914000	B, V
J0428-3756	04:28:40.8	-37:56:13	2.01±0.04	2.55±0.06	2.94±0.14	3.44±0.13	3.17±0.07	1.85±0.09	1.72±0.09	1.66±0.08	1.110000	B
J0450-8101	04:50:40.1	-81:01:05	0.95±0.04	1.13±0.05	1.29±0.09	1.73±0.10	1.75±0.05	1.45±0.16	1.20±0.06	1.07±0.05	0.444000	B
J0455-4616	04:55:53.0	-46:16:30	1.02±0.07	1.31±0.09	1.79±0.15	2.01±0.12	2.63±0.06	4.16±0.21	3.61±0.18	2.61±0.13	0.852800	B
J0457+0640	04:57:14.6	06:40:41	0.55±0.05	0.83±0.08	1.09±0.18	...	0.80±0.10	...	0.43	0.62	0.405000	B
J0525-2336	05:25:04.8	-23:36:40	0.42±0.03	0.65±0.07	...	1.37±0.16	1.13±0.06	0.79±0.05	0.89±0.05	0.81±0.04	3.100000	B
J0526-4831	05:26:00.7	-48:31:08	0.39±0.06	0.65±0.07	...	1.96±0.12	1.30±0.06	0.29±0.01	0.34±0.02	0.37±0.02	...	B
J0534-6107	05:34:36.7	-61:07:26	...	0.52±0.03	...	0.83±0.10	0.79±0.04	0.44±0.02	0.45±0.02	0.44±0.02	1.997000	B
J0538-4405	05:38:54.7	-44:05:13	6.67±0.07	8.45±0.06	9.32±0.13	8.46±0.13	9.00±0.07	5.29±0.25	4.23±0.21	3.80±0.19	0.894000	B, V
J0540-5418	05:40:57.1	-54:18:29	0.43±0.03	0.72±0.05	0.97±0.10	1.10±0.08	1.06±0.05	1.13±0.06	0.99±0.05	0.71±0.04	1.185000	B
J0550-5732	05:50:07.0	-57:32:06	0.60±0.02	0.74±0.04	1.01±0.07	1.54±0.08	1.45±0.05	1.00±0.05	1.03±0.05	0.93±0.05	2.001000	B
J0622-6435	06:22:55.9	-64:35:17	0.53±0.03	0.76±0.03	0.86±0.06	1.07±0.07	0.99±0.03	0.72±0.04	0.84±0.04	0.87±0.04	0.128889	B
J0639+7324	06:39:10.1	73:24:29	0.90±0.04	1.27±0.06	1.39±0.13	1.14±0.19	0.81±0.06	...	0.73	0.71	1.850000	B
J0646+4451	06:46:31.7	44:51:58	0.98±0.06	1.27±0.09	1.86±0.19	1.75±0.18	2.62±0.08	...	2.26	1.22	3.396000	B, V
J0701-4633	07:01:44.2	-46:33:29	0.66±0.03	0.86±0.04	1.02±0.09	1.34±0.08	1.05±0.05	1.07±0.05	0.86±0.04	0.55±0.03	0.822000	B
J0717+4539	07:17:50.2	45:39:47	0.38±0.06	...	0.98±0.14	...	0.95±0.08	...	0.56	0.47	0.940000	B
J0750+1231	07:50:50.4	12:31:34	2.04±0.03	2.69±0.07	3.18±0.15	3.90±0.15	4.54±0.08	...	1.97	1.24	0.889000	B, V
J0754+4820	07:54:48.0	48:20:17	0.65±0.07	0.94±0.08	0.90±0.17	...	0.69±0.09	...	0.20	0.23	0.377142	B
J0836-2237	08:36:52.3	-22:37:01	0.39±0.06	0.48±0.08	0.80±0.12	...	1.40±0.07	0.46±0.03	0.35±0.02	0.31±0.01	0.837000	B
J0841+7053	08:41:12.2	70:53:24	2.10±0.04	2.91±0.07	3.56±0.14	3.17±0.12	2.82±0.06	...	1.75	2.34	2.172000	B
J0847-0659	08:47:52.6	-06:59:02	0.54±0.05	0.92±0.06	0.99±0.14	...	0.91±0.06	0.73±0.04	0.47	0.44	...	B
J0854+2006	08:54:43.9	20:06:04	5.40±0.09	6.26±0.08	6.49±0.16	7.34±0.16	7.16±0.08	...	3.41	2.91	0.306000	B
J0920+4441	09:20:58.8	44:41:13	1.43±0.06	1.39±0.07	1.81±0.15	2.15±0.15	2.29±0.08	...	1.37	1.09	2.189910	B
J0923+2817	09:23:54.0	28:17:13	0.78±0.05	0.94±0.08	...	1.44±0.16	1.18±0.07	...	0.22	0.35	0.743902	B
J1102+7226	11:02:04.1	72:26:42	0.42±0.04	0.65±0.05	0.92±0.11	1.62±0.12	1.51±0.06	...	0.37	0.86	1.460000	B
J1147+4000	11:47:01.0	40:00:36	0.59±0.04	0.82±0.06	0.91±0.11	1.31±0.12	1.14±0.05	...	0.58	0.84	1.088000	B
J1152-0842	11:52:16.1	-08:42:40	0.75±0.05	1.13±0.09	1.25±0.21	...	1.41±0.08	0.67±0.03	0.56	0.74	2.370000	B
J1153+4930	11:53:18.0	49:30:14	1.16±0.06	1.53±0.06	1.60±0.12	1.73±0.11	1.80±0.05	...	0.44	0.17	0.333981	B
J1310+3221	13:10:26.2	32:21:50	1.30±0.06	1.56±0.09	2.27±0.18	2.96±0.16	3.58±0.08	...	3.03	1.45	0.996000	B, V
J1332-0509	13:32:09.6	-05:09:14	0.84±0.04	1.00±0.09	...	1.66±0.32	1.30±0.10	0.68±0.03	0.63	0.47	2.150000	B
J1337-1256	13:37:40.1	-12:56:46	2.77±0.06	3.40±0.10	3.79±0.23	4.48±0.24	4.32±0.10	6.06±0.29	5.00	2.84	0.539000	B, V
J1457-3543	14:57:24.7	-35:43:19	0.51±0.04	0.76±0.07	0.84±0.16	1.59±0.17	1.18±0.08	0.90±0.05	0.88±0.04	0.93±0.05	1.424000	B
J1506+4237	15:06:52.1	42:37:26	0.41±0.04	0.60±0.07	...	1.00±0.18	0.58±0.06	...	0.41	0.41	0.587000	B
J1516+0014	15:16:37.0	00:14:06	1.00±0.05	1.12±0.09	1.34±0.18	2.29±0.20	1.71±0.08	...	0.96	1.59	0.052489	B
J1549+0237	15:49:28.1	02:37:34	1.14±0.04	1.29±0.08	1.50±0.17	2.22±0.16	1.78±0.07	...	0.92	1.11	0.414414	B, V
J1553+1255	15:53:06.0	12:55:08	0.38±0.05	0.60±0.07	...	1.57±0.23	0.96±0.07	...	0.41	0.74	1.290000	B
J1604+5714	16:04:45.8	57:14:35	0.26±0.04	0.46±0.06	...	1.02±0.07	0.91±0.03	...	0.49	0.33	0.720000	B
J1635+3807	16:35:16.3	38:07:34	2.66±0.05	3.51±0.08	3.86±0.13	4.57±0.15	3.96±0.07	...	2.40	3.22	1.813570	B

Table 4. GPS source candidates in the ERCSC—*Continued*

Name	RA	Dec	$S_{143\text{ GHz}}$ [Jy]	$S_{100\text{ GHz}}$ [Jy]	$S_{70\text{ GHz}}$ [Jy]	$S_{44\text{ GHz}}$ [Jy]	$S_{30\text{ GHz}}$ [Jy]	$S_{20\text{ GHz}}$ [Jy]	$S_{8.6\text{ GHz}}$ [Jy]	$S_{4.8\text{ GHz}}$ [Jy]	Redshift	Notes
J1644–7716	16:44:32.4	–77:16:05	0.56±0.05	0.77±0.08	0.87±0.16	...	0.90±0.08	0.40±0.02	0.24±0.01	0.25±0.01	0.042700	B
J1703–6213	17:03:39.4	–62:13:08	0.96±0.04	1.33±0.07	1.48±0.16	2.67±0.14	2.24±0.08	1.05±0.05	1.03±0.05	1.04±0.05	...	B
J1727+4530	17:27:33.6	45:30:14	0.75±0.03	0.94±0.05	1.10±0.11	1.19±0.14	1.38±0.05	...	1.36	0.94	0.717000	B
J1927+7358	19:27:51.6	73:58:37	2.42±0.04	3.28±0.05	3.82±0.10	4.94±0.11	5.01±0.05	...	3.70	3.63	0.302100	B
J2005–1821	20:05:15.6	–18:21:04	0.46±0.05	0.62±0.08	0.98±0.17	...	1.18±0.09	0.60±0.03	0.42±0.02	0.40±0.02	0.868000	
J2006+6424	20:06:17.8	64:24:07	0.36±0.07	0.49±0.08	0.78±0.13	1.14±0.11	1.13±0.06	...	0.96	0.72	1.574000	B
J2009+7229	20:09:58.1	72:29:06	0.49±0.04	0.86±0.06	1.24±0.10	0.90±0.10	0.68±0.04	...	0.79	0.91	...	B
J2035–6845	20:35:25.0	–68:45:04	0.51±0.06	0.65±0.08	0.90±0.14	1.35±0.17	1.02±0.07	0.47±0.02	0.37±0.02	0.41±0.02	1.084000	B
J2100–2932	21:00:57.1	–29:32:02	0.51±0.04	0.71±0.07	1.02±0.15	1.17±0.21	0.62±0.10	0.39±0.02	0.48±0.02	0.56±0.03	1.492000	B
J2126–4607	21:26:36.5	–46:07:41	0.44±0.06	0.69±0.08	...	1.24±0.17	1.04±0.07	0.55±0.03	0.64±0.03	0.69±0.03	1.670000	B
J2139+1424	21:39:08.6	14:24:14	0.39±0.06	0.73±0.08	1.30±0.17	2.48±0.13	2.64±0.06	...	2.27	1.07	2.427000	B
J2147–7536	21:47:06.7	–75:36:40	2.12±0.04	2.48±0.06	3.09±0.14	3.37±0.12	2.93±0.06	0.49±0.03	0.86±0.04	1.01±0.05	1.139000	B
J2225+2119	22:25:36.0	21:19:23	1.10±0.05	1.19±0.08	1.28±0.12	2.16±0.15	1.87±0.06	...	1.40	1.02	1.959000	B
J2230–3940	22:30:45.6	–39:40:19	0.45±0.06	0.72±0.07	1.06±0.14	...	0.90±0.06	...	0.53	0.56	0.318049	B
J2235–4836	22:35:01.7	–48:36:32	0.62±0.04	0.93±0.05	1.07±0.12	1.19±0.14	1.32±0.06	1.99±0.09	2.07±0.10	1.21±0.06	0.510000	B
J2239–5701	22:39:16.3	–57:01:55	0.80±0.04	1.02±0.06	1.33±0.13	2.03±0.13	1.99±0.06	0.93±0.05	1.01±0.05	0.85±0.04	...	B
J2253+1609	22:53:59.8	16:09:07	27.94±0.16	28.83±0.14	27.91±0.29	22.75±0.20	16.84±0.10	...	10.38	14.47	0.859000	B

^(a) The 143 to 30 GHz flux densities of these sources are from the ERCSC (Planck Collaboration 2011c). The 20 GHz flux density is from the AT20G catalogue (Murphy et al. 2010). If a source is in the AT20G catalogue, its 8.6 GHz and 4.8 GHz flux densities are from the AT20G catalogue. If not, the 8.6 GHz flux density (8.4 GHz to be accurate) and 4.8 GHz flux densities are obtained from the CRATES catalogue (Healey et al. 2007). Note that the CRATES catalogue does not provide flux uncertainties. The tabulated redshift values are from the NASA/IPAC Extragalactic Database (NED).

^(b) In the “Notes” column, “B” indicate sources in the Roma-BZCAT blazar catalogue (Massaro et al. 2008) and CGRaBS blazar catalogue (Healey et al. 2008), “V” means these sources are found to be variable in Tornaiainen et al. (2005).

^(c) Source J2253+1609 is the well known quasar 3C454.3 that only shows GPS-like spectrum during strong flares (Rachen et al. 2010). See also discussion in § 5.2.

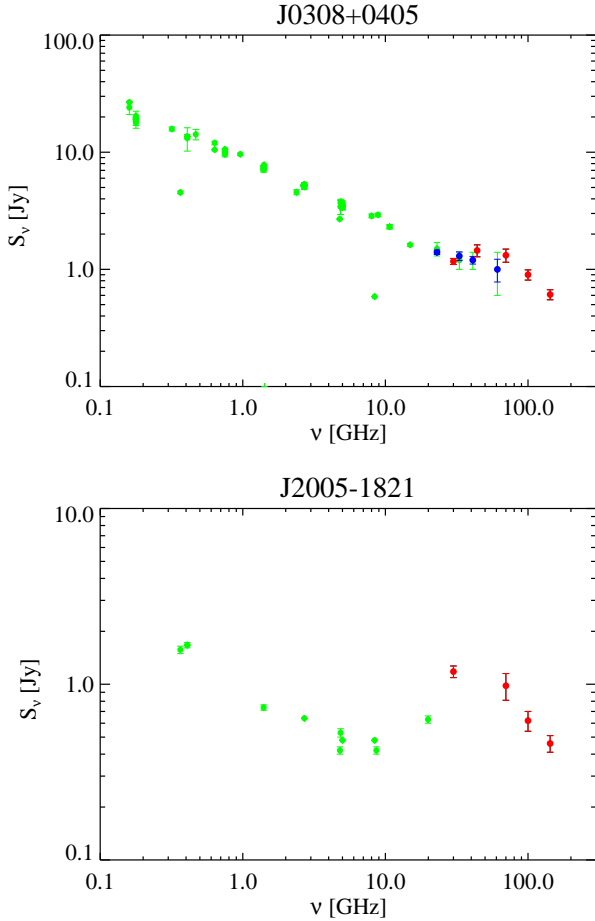


Fig. 7. SED plots of J0308+0405 (upper) and J2005–1821 (lower). *Planck* data are in red, *WMAP*-7yr data (if available) are in blue, archival data obtained from NED are in green.

5.1.3. Broad-peaked radio sources

As noted above, many sources showing GPS-like features are radio sources with dominant compact jet emission, usually identified with blazars. At VLBI resolution, they generally appear as one-sided, compact, jet-like objects. The most likely explanation for the very flat, sometimes inverted, radio spectra of these sources is the overlay of synchrotron-self absorbed emission in a continuous jet (Marscher 1977; Marscher & Gear 1985). We may note at this point that the application of this mechanism to a standard Blandford-Königl plasma jet (Blandford & Königl 1979) yields an optically thick spectral index $\alpha \approx 0.3-0.5$, depending on the electron spectral index (Marscher & Gear 1985). The turnover to a completely optically thin spectral index $\alpha < 0$, which is expected to happen somewhere in the GHz-THz regime from jet-size considerations, would then naturally produce a “GPS type” spectrum. We may therefore conclude that GPS-type blazars agree better with the simplest model of compact, continuous jets than do “typical” blazars which show a low frequency spectral index $\alpha \approx 0$ (Planck Collaboration 2011e).

Most of these objects are known to be strongly variable, on time scales down to one day (usually on week-month scale in the millimeter-regime, however). Variability and one-sided VLBI morphology give strong arguments in favor of beaming, i.e., the emission is strongly Doppler boosted, making the measured flux of the source at a given frequency depend on the Doppler fac-

tor D as $D^{3-\alpha}$. Therefore, small changes in the Doppler boosting, as expected in helix-shaped or precessing jets, can lead to strong variability. The flux density changes would be expected to be achromatic, i.e., leaving the spectral shape unchanged. This can be distinguished from variability due to distortions in the jet, which is expected to be emphasised in a specific frequency range; such sources are discussed in § 5.2.

Figure 8 shows two examples of apparently achromatic variability: J1800+7828 shows a rather typical GPS blazar spectrum, with $\alpha \approx 0.3$ below the peak frequency at about 10 GHz, and steepening to $\alpha \approx -0.17$ for $\nu \leq 100$ GHz, with a further break to $\alpha \approx -0.5$ at still higher frequencies; The more dome-like spectrum of J0423–0120, with $\alpha \approx 1$ at lower frequencies, points to a more uniform component producing the radiation. Supporting, ground-based, radio data from Effelsberg, Metsähovi and the VLA further suggest significant, achromatic variability for this source, as would be expected from changes of the Doppler boosting in a helical or precessing jet. The high frequency spectrum has the same characteristics as J1800+7828. The temporarily very flat index $\alpha \approx -0.2$ after the peak may suggest an unusually flat electron spectrum, as discussed in Planck Collaboration (2011e).

5.2. Flat and multi-component spectra

In our examination of radio sources in the ERCSC we found a large number with extended, flat, power law spectra. For instance, the flux density of J2203+1725, as determined by *Planck* and VLA observations, varies only between 0.99 and 1.18 Jy between frequencies of 4.9 and 100 GHz, and decreases only to 0.906 Jy at 143 GHz. Many of these flat spectrum sources are the blazars discussed in Planck Collaboration (2011e). We also found several sources with prominently zig-zag or “bumpy” spectra. In some cases the variation in flux density from one *Planck* band to the next was several times the associated errors. This could result from the superposition of emission from several components, as is probably the case in the examples shown in Figure 9. However, it is important to recall that *Planck*’s multi-frequency observations were not exactly simultaneous. A source could sweep through the *Planck* beams at one frequency days before doing so at a neighboring frequency (depending on position, it takes 7-10 days for a source to drift entirely across the focal plane). Hence fast variability on time-scales of days can contribute to irregularities in its *Planck* spectrum. We expect this effect to be smaller for the HFI frequencies, given the relatively closer packing in the focal plane. We discuss below the possible physical conditions for true multi-component sources, followed by examples of spectral artifacts caused by variability.

5.2.1. Flat spectrum sources with a variable component

Spectra resulting from superposed radiation of at least two components have become the standard model to explain flaring blazars; this is known as a “shock-in-jet” model (Marscher & Gear 1985). One component, the jet, produces a flat ($\alpha \sim 0$) spectrum up to some break frequency, mostly between ~ 10 and ~ 100 GHz, above which the spectrum steepens to a typical index $\alpha \sim -0.7$. The second component, associated with an evolving shock, produces a self-absorbed synchrotron spectrum with a turnover frequency ~ 100 GHz. Below this turnover frequency, the spectrum is strongly inverted. As the shock evolves, the turnover frequency and the flux density of the shock component

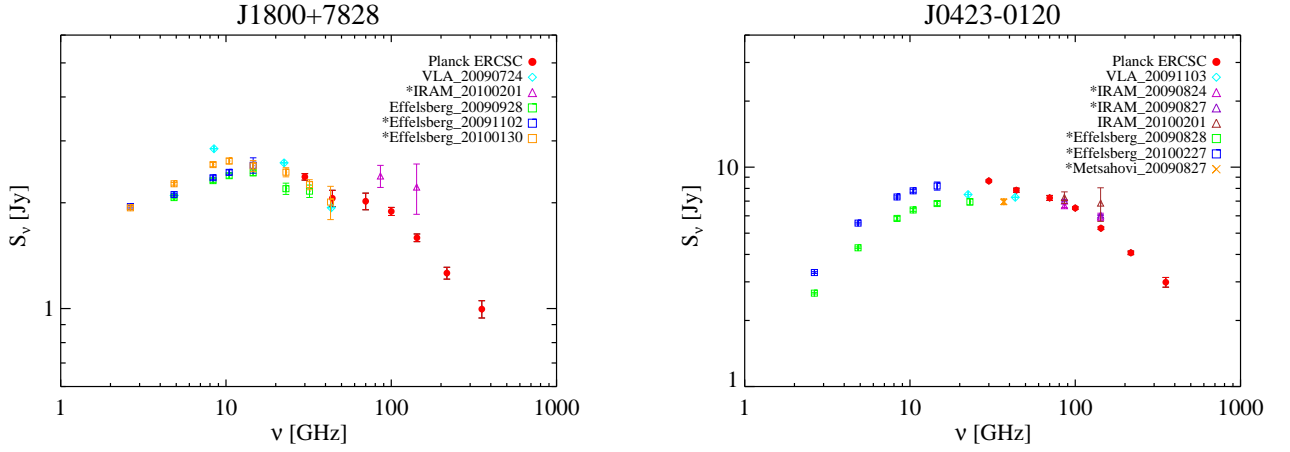


Fig. 8. VLA, Metsähovi, IRAM, Effelsberg and *Planck* measurements of two known GPS blazars: J1800+7828 (left) and J0423–0120 (right). While the former shows only small signs of variability, the latter is clearly variable while preserving its spectral shape, pointing to helical or pressing jet (see text). Asterisks identify epochs within 10 days from *Planck* observations at any of the LFI channels. For both sources, the *Planck* ERCSC data are a superposition of two scans separated by 3 and 6 months, respectively.

changes, and in some phases a detectable contribution of this component may not be present at all.

An example of this class is J2253+1609, better known as 3C454.3. During an outburst in 2005/2006, the source showed a strong spectral peak around 300 GHz, evolving to lower frequencies over several months, while observations made in 2004 did not show this feature (see Villata et al. 2007, Raiteri et al. 2008, Villata et al. 2009, Rachen et al. 2010 and references therein). Incidentally, this source showed a similar outburst when it was first observed with *Planck* (Planck Collaboration 2011e), which is why it is included in Table 4. Two other examples where *Planck* observations play a crucial role are shown in Figure 9. The sources shown in Figure 5, all identified with known blazars, present a very similar spectral shape. We therefore expect that their high-frequency-peaked spectrum is a temporary feature.

We emphasise that *Planck*, which is expected to perform at least four full sky surveys, is a powerful tool to distinguish variable from permanent spectral features. By comparing catalogues derived from individual surveys made by *Planck*, we will be able to resolve the questions raised here in the full frequency regime accessible to *Planck*, even without reference to external data. Results from this research will be presented in future *Planck* papers.

5.2.2. Artifacts in the ERCSC spectra of variable sources

In this subsection, we discuss some potential problems in interpreting ERCSC spectra for variable sources. As noted in § 1, 44 GHz observations of a given source take place at two times separated by 7–10 days, for each scan. If the source is strongly variable on a time scale of order days, the 44 GHz flux density contained in the ERCSC could be an awkward average. An example is the well-known, rapidly variable sources J0722+7120 (Ostorero et al. 2006), shown in Figure 10. Supporting observations, particularly the IRAM data at 86 and 143 GHz, show it to have varied on short time scales during the *Planck* survey. The apparently anomalous 44 GHz *Planck* measurement is an average of the flux density in the source’s high and low luminosity state. We show this case as a warning: spectral anomalies seen only at 44 GHz may be due to this effect.

In sources with still faster variability, the effect of non-simultaneity of the *Planck* observations can produce even more bizarre effects. The ERCSC spectrum of the source J1159+2914, also known as the IDV blazar TON599, shows a strong zig-zag shape, dropping by a factor of two between 44 and 70 GHz, followed by another small bump (see Figure 11). This source is known to show very fast variability, and the comparison with Effelsberg data, and IRAM 86 GHz and 143 GHz data taken around the time of the *Planck* scans, suggests that it had a strong flare at a peak frequency of ~50 GHz in the first days of June 2010. This flare must have started after 23 May (when the Effelsberg observations were made), and probably declined again on 7 June when the *Planck* 100 GHz point was taken. The ERCSC spectrum of the source is a superposition of a quite low state in December 2009, and the high, flaring state in June 2010, except for 30 and 70 GHz measurements, which were made by *Planck* for the second time shortly after the last day of data used for ERCSC, and are therefore not included in the average.

These examples make clear that a fair amount of care has to be taken when interpreting *Planck* ERCSC spectra for variable sources.

5.3. Sources showing evidence of a spectral upturn at high frequency

In many radio sources (Arp 220 as an example), synchrotron emission is dominated at high frequencies by re-emission from warm dust. As already noted, essentially no extragalactic *Planck* sources show this pattern at frequencies below 143 GHz. Of all the sources at $|b| > 30^\circ$ that have *Planck* measurements at 30 to 217 GHz, only eleven show evidence of a significant increase of flux density even from 143 GHz to 217 GHz; one of these is the nearby and well-studied star-forming galaxy NGC253 (Figure 12). Of the remaining 10 sources, 7 are HII regions located in the Magellanic clouds, like J0047–7310 and J0048–7306; two are Galactic sources; and the remaining one is M82, a well-known starburst galaxy. The lack of upturn-spectrum sources in the ERCSC suggests that most of the sources detected by *Planck* are flat spectrum sources like blazars, with high enough synchrotron luminosity to swamp dust reemission even up to 217 GHz.

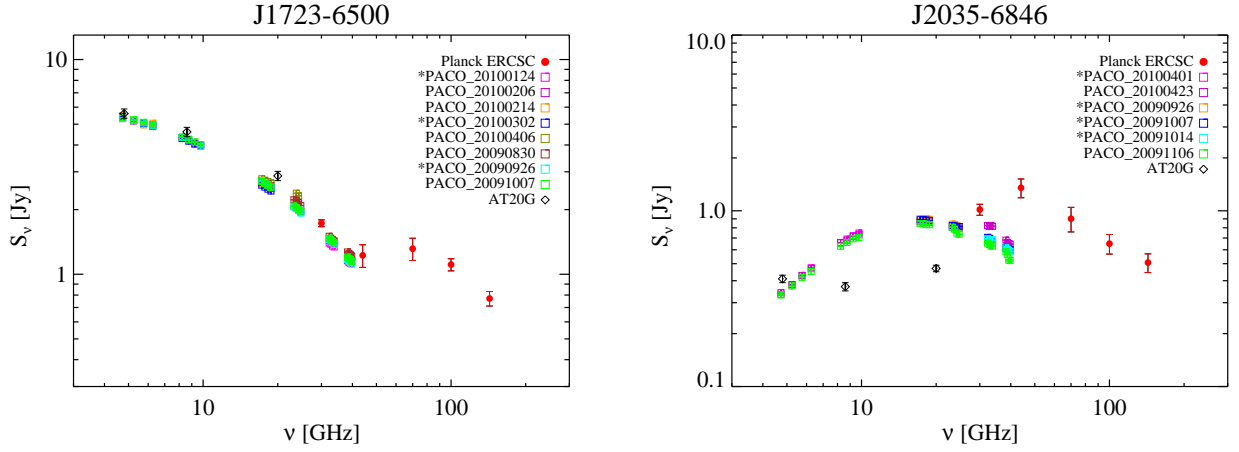


Fig. 9. Two examples of clearly multi-component spectra. *Planck* measurements are in filled circles; AT20G data are in open diamonds; PACO data, with their dense sampling in frequency space, are shown in open squares. Asterisks identify epochs within 10 days from *Planck* observations. The multi-valued spectra in J2035–6846 are a clear sign that this source is variable on time scales less than two weeks (see text).

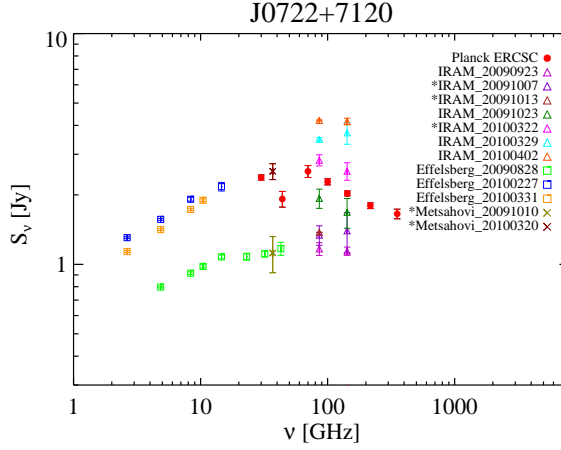


Fig. 10. Based on ground-based and *Planck* data, the apparently anomalous 44 GHz point in the spectrum of the strongly variable source J0722+7120 is shown to be due to the averaging of flux densities described in § 5.2.2. Asterisks identify epochs within 10 days from *Planck* observations at any of the LFI channels.

We also note here the potential danger of apparently upturning spectra being produced by source confusion. The low probability of source confusion discussed in § 4.1 is valid only for the low frequency catalogues; at 545 and 857 GHz, in particular, the ERCSC catalogues are much richer, and these frequencies are in the Rayleigh-Jeans part of the spectra for most IR sources. The apparently upturning spectra may result from confusion of a radio source disappearing in the background with an IR source appearing within the large beam of *Planck*. Careful checks with infrared catalogues are required to verify any case of a potentially upturning spectrum. Hence we restrict our attention in this paper to frequencies of 30–353 GHz, and generally to 30–217 GHz.

5.4. ERCSC LFI sources with no plausible match in existing radio catalogues

Finally, we looked for sources with such extreme spectra that they have no counterparts in existing low-frequency, large area, radio surveys. This serves the dual purpose of looking for unusual or extreme sources and validating the ERCSC. We looked for matches in the following catalogues: the WMAP 7 year

catalogue (Gold et al. 2011), the NEWPS catalogue (Massardi et al. 2009), the 20 GHz AT20G survey in the southern hemisphere (Murphy et al. 2010), the CRATES catalogue in the northern hemisphere (Healey et al. 2007), and the GB6 catalogue (Condon et al. 1994). To reduce the number of spurious identifications of the bright *Planck* sources, a flux density cut of 0.3 Jy was applied to both the AT20G and GB6 catalogues. In the northern hemisphere, where the high frequency coverage is incomplete, we also looked at the 1.4 GHz NVSS catalogue (Condon et al. 1998) with a 0.5 Jy flux density cut. We cross-correlated these catalogues with the ERCSC at 30 GHz, 44 GHz and 70 GHz using a search radius equal to 0.5 FWHM at each *Planck* frequency channel. We have shown in § 4 that this search radius is unlikely to yield spurious matches. We also experimented with different flux cuts, but found that our adopted cuts are reasonable compromises between matching most sources and avoiding spurious matches. Significantly lower flux cuts result in spurious matches because the chance of random association given the large LFI beams goes up. The unmatched sources listed in Table 5 for example often have NVSS sources within the *Planck* LFI beams, but the 1.4 GHz flux densities of these NVSS

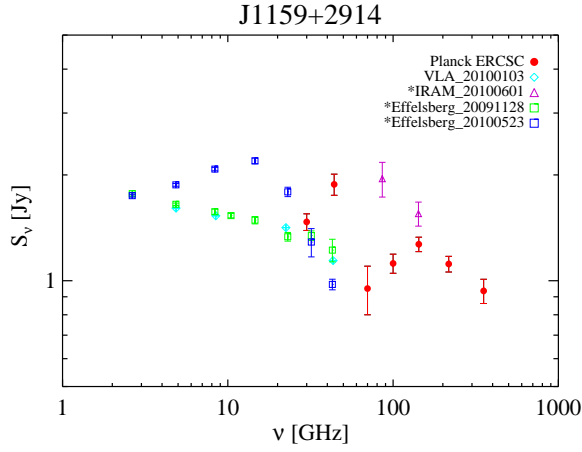


Fig. 11. The zig-zag shape spectrum of the strongly variable source J1159+2914. Asterisks identify epochs within 10 days from *Planck* observations at any of the LFI channels.

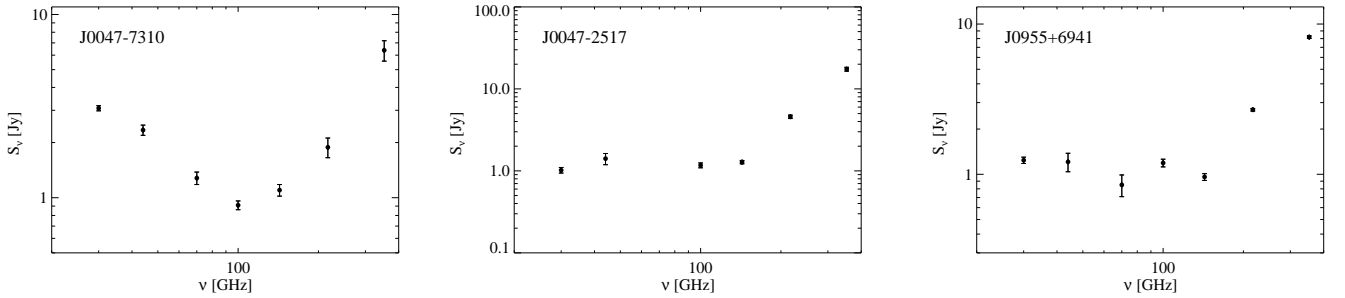


Fig. 12. *Planck* sources with an upturn in the spectrum. *Left:* J0047–7310 in the SMC. *Center:* *Planck* spectrum of a familiar star-forming system, NGC253. *Right:* The starburst galaxy M82.

sources are on the order of a few mJy; thus they are clearly unlikely to be associated with the ERCSC sources, whose flux densities are on the order of 1 Jy or above.

With these automatic matching steps, we found that among high Galactic latitude ($|b| > 5^\circ$) sources, 12 ERCSC sources at 30 GHz, 13 at 44 GHz and 26 at 70 GHz do not match with any known source. These represent respectively 2%, 5% and 8% of the high Galactic latitude sources in each of these catalogues. However, there is a caveat in such automatic matching procedure. While the above matching radius is reasonable assuming that *Planck* dominates the positional uncertainty, this is not necessarily the case, for example, when matching against the WMAP sources. The comparatively smaller beam sizes at 44 and 70 GHz of *Planck* suggest that this procedure could miss genuine WMAP matches.

Since sources that exist in only one *Planck* channel are more likely spurious, we first looked for unmatched sources that exist in more than one *Planck* band, and found a number of such cases among the 44 and 70 GHz “unmatched” sources. We then looked in NED for each of these unmatched sources to see if they have counterparts in other radio catalogues that are not among those listed above. In particular, extended sources may appear in older, lower resolution surveys such as PMN (Griffith & Wright 1993), but not in newer, higher resolution surveys such as AT20G. Several such cases were found. We further associated a number of unmatched sources with Galactic objects such as PNe and SNR. After these checks, the number of residual, apparently unmatched sources is 5 at 30 GHz, 6 at 44 GHz, and 15 at 70 GHz. These are listed in Table 5. Judging from the

Galactic latitude, 2 of the 30 GHz, 3 of the 44 GHz and 4 of the 70 GHz sources are likely associated with the Galaxy while one of the 70 GHz sources is likely in the LMC; these are flagged in Table 5. The remaining sources are either exciting “new” sources or else spurious. To distinguish between these possibilities, we looked at the postage stamp images for all the sources that remain unidentified (see Figure 13). In all cases, the postage stamps are 5 FWHM on a side. A number of the sources at 44 and 70 GHz appear to be of low significance and hence could be spurious. Some are flagged in the ERCSC as possibly contaminated by CMB signals. Others are at low Galactic latitude. One apparent exception at 70 GHz is G158.33–20.53 (but see comments below). At 30 GHz, some sources are of high significance but appear extended, which, given the $\sim 30'$ *Planck* beam size, means they are likely to be either Milky Way objects or associated with very nearby galaxies (or could be CMB artifacts). An exception is G219.17–08.90 ($S_{30\text{ GHz}} = 1\text{ Jy}$) which appears to be real and point-like. From NED, we find that there is a $S_{60\text{ }\mu\text{m}} = 68\text{ Jy}$ IRAS source (IRAS06282–0935) near this position that seems to have been identified as IR cirrus (Strauss et al. 1992). The most convincing 70 GHz source, G158.33–20.53, also has a counterpart, IRAS03259+3105, in NED, which again is identified as cirrus by Strauss et al. (1992).

We thus conclude that we do not identify any genuinely new population of sources among the ERCSC catalogues at the LFI frequencies. While confirming a match is generally much easier than claiming a source is “unmatched”, we can say that after the automated procedure described above, $> 90\%$ of the LFI sources had a reasonable match in an external radio catalogue.

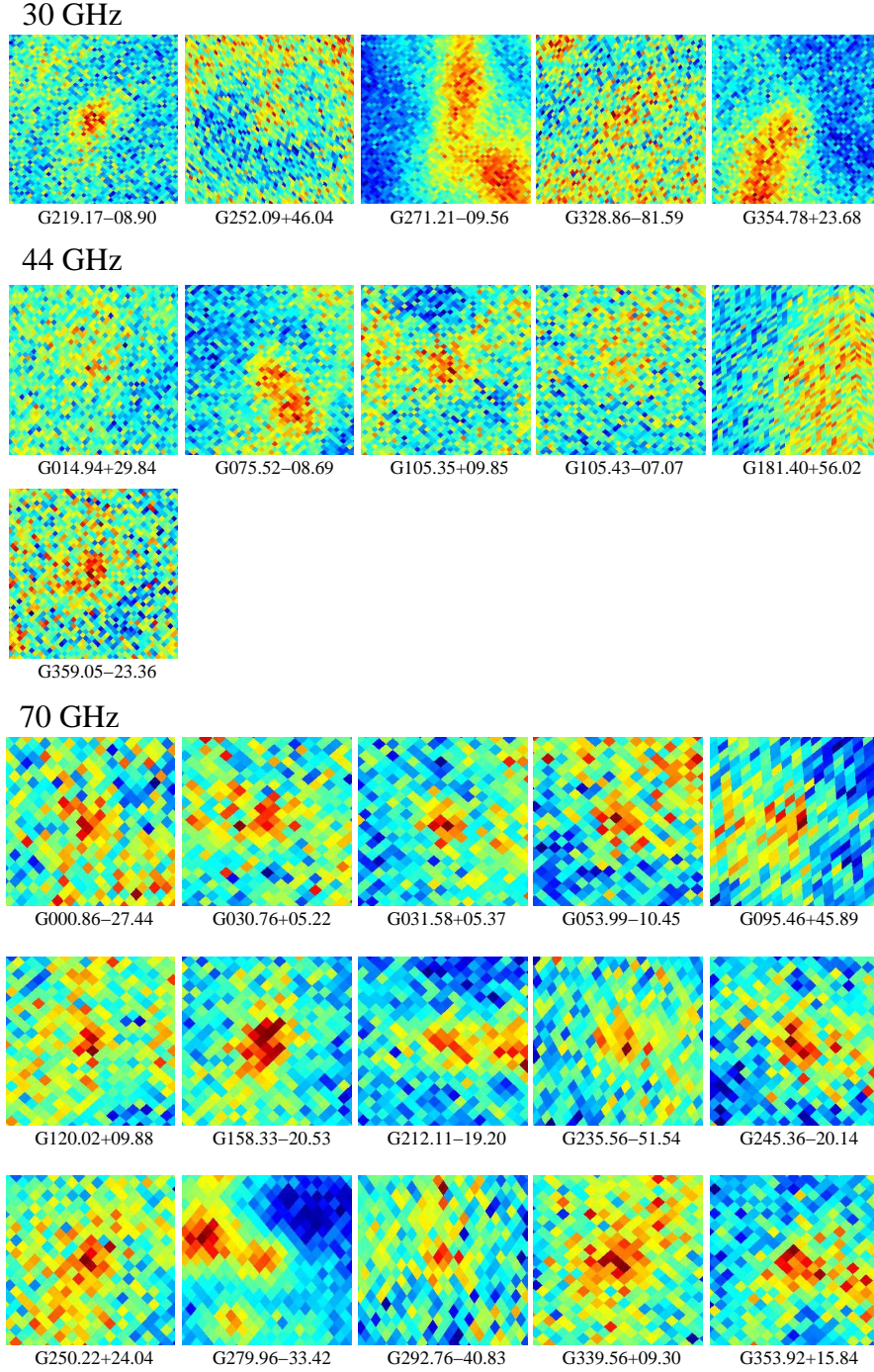


Fig. 13. ERCSC sources with no plausible identifications in low frequency radio catalogues.

After cross-matching between the three LFI bands and searching in NED for plausible identifications, especially important in the case of extended radio sources, we are left with a total of 26 potentially “unidentified” LFI sources, almost all of which can probably be explained by artifacts or extended Galactic structures.

6. Conclusions

We summarise in this section the primary conclusions to be drawn from *Planck*’s study of extragalactic radio sources. We stick closely to the observational results, and provide comments

on the fit between these observational results and current theories of the physics of extragalactic radio sources.

6.1. Overall properties

Planck has demonstrated that the high frequency counts (at least for frequencies ≤ 143 GHz) of extragalactic sources are dominated at the bright end by synchrotron emitters, not dusty galaxies. This finding is in agreement with conclusions reached by the South Pole Telescope (SPT) and Atacama Cosmology Telescope (ACT) teams (Vieira et al. 2010; Marriage et al. 2010, respectively) from the properties of sources at much lower flux densities. An inference from this result is that the cores of extra-

Table 5. ERCSC sources at $|b| > 5^\circ$ with no obvious match in external radio catalogues

ERCSC Name	Notes*
PLCKERC030 G219.17–08.90	G
PLCKERC030 G252.09+46.04	
PLCKERC030 G271.21–09.56	G
PLCKERC030 G328.86–81.59	
PLCKERC030 G354.78+23.68	G
PLCKERC044 G014.94+29.84	
PLCKERC044 G075.52–08.69	G
PLCKERC044 G105.35+09.85	G
PLCKERC044 G105.43–07.07	G
PLCKERC044 G181.40+56.02	
PLCKERC044 G359.05–23.36	
PLCKERC070 G000.86–27.44	G?
PLCKERC070 G030.76+05.22	G
PLCKERC070 G031.58+05.37	G?
PLCKERC070 G053.99–10.45	G
PLCKERC070 G095.46+45.89	
PLCKERC070 G120.02+09.88	G
PLCKERC070 G158.33–20.53	G?
PLCKERC070 G212.11–19.20	
PLCKERC070 G235.56–51.54	
PLCKERC070 G245.36–20.14	
PLCKERC070 G250.22+24.04	
PLCKERC070 G279.96–33.42	L?
PLCKERC070 G292.76–40.83	
PLCKERC070 G339.56+09.30	G
PLCKERC070 G353.92+15.84	G?

* Here G stands for likely Galactic source. L stands for likely LMC source.

galactic sources, and not extended structure, dominate the high frequency emission, as suggested by earlier work at frequencies below most of the *Planck* bands (see recent discussions in Lin et al. 2009 and Murphy et al. 2010). The conclusion that the core dominates the high frequency emission is supported by the close agreement between *Planck* and VLA flux densities (§ 4), implying that the emission is found within the VLA beam of order arcseconds in size.

The emerging dominance of emission from a flat spectrum core implies that extrapolation of flux densities and/or counts of sources to frequencies ≥ 30 GHz cannot be reliably made from low frequency catalogues, where the emission is dominated by lobes. This has been recognised for some time (see Lin et al. (2009) and Murphy et al. (2010)); *Planck* strongly confirms this conclusion. If we look at the SEDs of the sources, including all components, the spectra grow flatter as frequency increases and the steep-spectrum lobes fade away. On the other hand, *Planck* observations allow us to follow the SEDs of a statistically significant sample of sources to much higher frequencies than can generally be employed in ground-based observations. As noted in § 4 (and described in more detail in Planck Collaboration 2011d), *Planck* provides clear evidence of a spectral steepening in the radio and millimeter wave emission from extragalactic cores; the steepening sets in at frequencies above ~ 44 –70 GHz. The observed spectral steepening in turn means that radio sources contribute less foreground noise to increasingly sensitive searches for small angular scale anisotropies in the CMB than earlier models had suggested (e.g., de Zotti et al. 2005). This finding, too, is consonant with results from SPT and ACT.

6.2. Properties of individual sources

Planck allows us for the first time to investigate sub-mm spectra beyond 200 GHz, which is the limit of most ground-based monitoring programs. In this regime, the spectra of radio sources are usually expected to be optically thin synchrotron emission, and our results largely confirm that this part of the spectrum is represented by a single power law. The vast majority of extragalactic sources in the ERCSC lists at 30–100 GHz are flat spectrum radio sources of the sort discussed in detail in Planck Collaboration (2011e), with a scattering of bright steep spectrum sources strong enough to register in the lowest frequency bands of *Planck*. A small fraction ($\lesssim 10\%$; Table 4) show peaked or convex spectra, but even these sources are mostly identified as known blazars. As blazars are known to be variable, care has to be taken in the interpretation of their spectra. For most sources, ERCSC flux densities represent the average over two scans, and even during one scan, spectral artifacts may occur due to the fact that it requires 7–10 days for the *Planck* focal plane to cross a point source.

In contrast, most known examples of compact, newborn radio galaxies (CSOs), which were originally thought to be the dominant class of sources with Gigahertz-peaked spectra, are mostly too faint to be detected by *Planck*. A new population of bright, very compact, high-peaked CSOs has not been found. Likewise, very few of the extragalactic radio sources found by *Planck* show evidence of the sharp spectral upturn expected from dust reemission at high frequencies. Only NGC253 shows a clear upturn at a frequency ≤ 143 GHz; sources that show dust reemission dominating at 217 GHz are in many cases Galactic sources, in the Magellanic clouds, or nearby known star-forming galaxies.

Although we have not investigated in detail all the sources with no obvious matches in lower frequency radio catalogues (§ 5.4), let alone every extragalactic source in the ERCSC, we find no convincing evidence for the emergence of a new and unexpected population of sources. The 26 ERCSC sources with no match in radio catalogues appear to be a heterogeneous mixture of conventional radio sources, many of them Galactic.

6.3. Future observations and analysis

Two sets of future observations will help clarify the status of some of the sources listed in § 5.1 and § 5.2. Careful monitoring and/or VLBI observations of sources with peaked spectra would determine whether they are highly compact radio galaxies (CSOs), compact jet objects with stable GPS type spectra, or are instead merely flaring sources with temporarily convex spectra. In fact, our results seem to suggest most extreme spectral features seen in *Planck* sources may be associated with flares. With at least four full sky surveys, *Planck* is a powerful tool to distinguish these possibilities, by deriving catalogues from individual, six-month, sky surveys and comparing flux densities of all bright point sources at six-month intervals. Further ground-based observations, now underway at frequencies below and overlapping the *Planck* frequency bands, will support this effort.

Likewise, for the non-variable extreme radio sources like CSOs, the addition of more surveys to the *Planck* maps will allow us to extract deeper catalogues, with the potential to find some more of these usually faint objects.

In the case of Galactic sources, the role of CO emission lines is important. The situation for extragalactic sources is more complicated, because the CO lines redshift in and out of the *Planck* bands. We have underway a study to look for the influence of

CO emission in the ERCSC spectra. We expect the effect to be small, since most of the ERCSC sources are extremely bright, non-thermal emitters, with strong continua. There is no obvious evidence in the SEDs we have examined for the presence of CO emission. In this regard, we again warn readers to be careful in interpreting anomalous 44 GHz observations; a spectral bump at 44 GHz is not necessarily evidence for redshifted CO.

We used ground-based observation data for both validation purposes, specifically cross-calibration between ground-based instruments and *Planck*, and in the study of the spectral and variability properties of extreme radio sources. Most of these observation programs, like the *Planck* mission itself, are still ongoing.

Acknowledgements. A description of the Planck Collaboration and a list of its members can be found at http://www.rssd.esa.int/index.php?project=PLANCK&page=Planck_Collaboration. This paper makes use of observations obtained at the Very Large Array (VLA) which is an instrument of the National Radio Astronomy Observatory (NRAO). The NRAO is a facility of the National Science Foundation operated under cooperative agreement by Associated Universities, Inc. This research also makes use of observations with the 100 m telescope of the Max Planck Institut für Radioastronomie (MPIfR), the 30 m telescope of Institut de Radioastronomie Millimétrique (IRAM), the Australia Telescope Compact Array (ATCA) and the 13.7 m telescope of the Metsähovi Radio Observatory. The Metsähovi observing project is supported by the Academy of Finland (grant numbers 212656, 210338 and 121148). We acknowledge the use of the NASA/IPAC Extragalactic Database (NED) which is operated by the Jet Propulsion Laboratory, California Institute of Technology, under contract with the National Aeronautics and Space Administration. The Planck Collaboration acknowledges the support of: ESA; CNES and CNRS/INSU-IN2P3-INP (France); ASI, CNR and INAF (Italy); NASA and DoE (USA); STFC and UKSA (UK); CSIC, MICINN and JA (Spain); Tekes, AofF and CSC (Finland); DLR and MPG (Germany); CSA (Canada); DTU Space (Denmark); SER/SSO (Switzerland); RCN (Norway); SFI (Ireland); FCT/MCTES (Portugal); and DEISA (EU).

References

- Angelakis, E., Fuhrmann, L., Marchili, N., Krichbaum, T. P., & Zensus, J. A. 2008, *Mem. Soc. Astron. Italiana*, 79, 1042
- Bersanelli, M., Mandolesi, N., Butler, R. C., et al. 2010, *A&A*, 520, A4+
- Bertin, E. & Arnouts, S. 1996, *A&AS*, 117, 393
- Blandford, R. D. & Königl, A. 1979, *ApJ*, 232, 34
- Bolton, R. C., Chandler, C. J., Cotter, G., et al. 2006, *MNRAS*, 367, 323
- Carvalho, P., Rocha, G., & Hobson, M. P. 2009, *MNRAS*, 393, 681
- Condon, J. J., Broderick, J. J., Seielstad, G. A., Douglas, K., & Gregory, P. C. 1994, *AJ*, 107, 1829
- Condon, J. J., Cotton, W. D., Greisen, E. W., et al. 1998, *AJ*, 115, 1693
- Conway, J. E. 2002, *New A Rev.*, 46, 263
- Dallacasa, D., Stanghellini, C., Centonza, M., & Fanti, R. 2000, *A&A*, 363, 887
- de Zotti, G., Ricci, R., Mesa, D., et al. 2005, *A&A*, 431, 893
- Fuhrmann, L., Krichbaum, T. P., Witzel, A., et al. 2008, *A&A*, 490, 1019
- Fuhrmann, L., Zensus, J. A., Krichbaum, T. P., Angelakis, E., & Readhead, A. C. S. 2007, in *American Institute of Physics Conference Series*, Vol. 921, *The First GLAST Symposium*, ed. S. Ritz, P. Michelson, & C. A. Meegan, 249–251
- Gold, B., Odegard, N., Weiland, J. L., et al. 2011, *ApJS*, 192, 15
- Griffith, M. R. & Wright, A. E. 1993, *AJ*, 105, 1666
- Healey, S. E., Romani, R. W., Cotter, G., et al. 2008, *ApJS*, 175, 97
- Healey, S. E., Romani, R. W., Taylor, G. B., et al. 2007, *ApJS*, 171, 61
- Hovatta, T., Niemppola, E., Tornikoski, M., et al. 2008, *A&A*, 485, 51
- Lamarre, J., Puget, J., Ade, P. A. R., et al. 2010, *A&A*, 520, A9+
- Leahy, J. P., Bersanelli, M., D’Arcangelo, O., et al. 2010, *A&A*, 520, A8+
- Lin, Y., Partridge, B., Pober, J. C., et al. 2009, *ApJ*, 694, 992
- Mandolesi, N., Bersanelli, M., Butler, R. C., et al. 2010, *A&A*, 520, A3+
- Marriage, T. A., Juin, J. B., Lin, Y., et al. 2010, *ArXiv e-prints*
- Marscher, A. P. 1977, *ApJ*, 216, 244
- Marscher, A. P. & Gear, W. K. 1985, *ApJ*, 298, 114
- Massardi, M., Bonaldi, A., Bonavera, L., et al. 2011, *ArXiv e-prints*
- Massardi, M. & Burigana, C. 2010, *New A*, 15, 678
- Massardi, M., López-Cañiego, M., González-Nuevo, J., et al. 2009, *MNRAS*, 392, 733
- Massaro, E., Giommi, P., Leto, C., et al. 2008, *Mem. Soc. Astron. Italiana*, 79, 262
- Mennella et al. 2011, *Planck early results 03: First assessment of the Low Frequency Instrument in-flight performance* (Submitted to *A&A*, [arXiv:astro-ph/1101.2038])
- Murphy, T., Sadler, E. M., Ekers, R. D., et al. 2010, *MNRAS*, 402, 2403
- Nieppola, E., Hovatta, T., Tornikoski, M., et al. 2009, *AJ*, 137, 5022
- O’Dea, C. P. 1998, *PASP*, 110, 493
- Ostorero, L., Wagner, S. J., Gracia, J., et al. 2006, *A&A*, 451, 797
- Owsianik, I. & Conway, J. E. 1998, *A&A*, 337, 69
- Planck Collaboration. 2011a, *Planck early results 01: The Planck mission* (Submitted to *A&A*, [arXiv:astro-ph/1101.2022])
- Planck Collaboration. 2011b, *Planck early results 02: The thermal performance of Planck* (Submitted to *A&A*, [arXiv:astro-ph/1101.2023])
- Planck Collaboration. 2011c, *Planck early results 07: The Early Release Compact Source Catalogue* (Submitted to *A&A*, [arXiv:astro-ph/1101.2041])
- Planck Collaboration. 2011d, *Planck early results 13: Statistical properties of extragalactic radio sources in the Planck Early Release Compact Source Catalogue* (Submitted to *A&A*, [arXiv:astro-ph/1101.2044])
- Planck Collaboration. 2011e, *Planck early results 15: Spectral energy distributions and radio continuum spectra of northern extragalactic radio sources* (Submitted to *A&A*, [arXiv:astro-ph/1101.2047])
- Planck HFI Core Team. 2011a, *Planck early results 04: First assessment of the High Frequency Instrument in-flight performance* (Submitted to *A&A*, [arXiv:astro-ph/1101.2039])
- Planck HFI Core Team. 2011b, *Planck early results 06: The High Frequency Instrument data processing* (Submitted to *A&A*, [arXiv:astro-ph/1101.2048])
- Rachen, J. P., Häberlein, M., Reimold, F., & Krichbaum, T. 2010, *ArXiv e-prints*
- Raiteri, C. M., Villata, M., Larionov, V. M., et al. 2008, *A&A*, 491, 755
- Rosset, C., Tristram, M., Ponthieu, N., et al. 2010, *A&A*, 520, A13+
- Sajina, A., Partridge, B., Evans, T., et al. 2011, *ApJ*, in press
- Strauss, M. A., Davis, M., Yahil, A., & Huchra, J. P. 1992, *ApJ*, 385, 421
- Tauber, J. A., Mandolesi, N., Puget, J., et al. 2010, *A&A*, 520, A1+
- Teraesranta, H., Tornikoski, M., Mujunen, A., et al. 1998, *A&AS*, 132, 305
- Torniaainen, I., Tornikoski, M., Teräsraanta, H., Aller, M. F., & Aller, H. D. 2005, *A&A*, 435, 839
- Tornikoski, M., Jussila, I., Johansson, P., Lainela, M., & Valtaoja, E. 2001, *AJ*, 121, 1306
- Vieira, J. D., Crawford, T. M., Switzer, E. R., et al. 2010, *ApJ*, 719, 763
- Villata, M., Raiteri, C. M., Aller, M. F., et al. 2007, *A&A*, 464, L5
- Villata, M., Raiteri, C. M., Gurwell, M. A., et al. 2009, *A&A*, 504, L9
- Vollmer, B., Krichbaum, T. P., Angelakis, E., & Kovalev, Y. Y. 2008, *A&A*, 489, 49
- Zacchei et al. 2011, *Planck early results 05: The Low Frequency Instrument data processing* (Submitted to *A&A*, [arXiv:astro-ph/1101.2040])

- 1 Aalto University Metsähovi Radio Observatory, Metsähovintie 114, FIN-02540 Kylmälä, Finland
- 2 Agenzia Spaziale Italiana Science Data Center, c/o ESRIN, via Galileo Galilei, Frascati, Italy
- 3 Astroparticule et Cosmologie, CNRS (UMR7164), Université Denis Diderot Paris 7, Bâtiment Condorcet, 10 rue A. Domon et Léonie Duquet, Paris, France
- 4 Astrophysics Group, Cavendish Laboratory, University of Cambridge, J J Thomson Avenue, Cambridge CB3 0HE, U.K.
- 5 Atacama Large Millimeter/submillimeter Array, ALMA Santiago Central Offices, Alonso de Cordova 3107, Vitacura, Casilla 763 0355, Santiago, Chile
- 6 Australia Telescope National Facility, CSIRO, P.O. Box 76, Epping, NSW 1710, Australia
- 7 CITA, University of Toronto, 60 St. George St., Toronto, ON M5S 3H8, Canada
- 8 CNRS, IRAP, 9 Av. colonel Roche, BP 44346, F-31028 Toulouse cedex 4, France
- 9 California Institute of Technology, Pasadena, California, U.S.A.
- 10 DAMTP, University of Cambridge, Centre for Mathematical Sciences, Wilberforce Road, Cambridge CB3 0WA, U.K.
- 11 DSM/Irfu/SPP, CEA-Saclay, F-91191 Gif-sur-Yvette Cedex, France
- 12 DTU Space, National Space Institute, Juliane Mariesvej 30, Copenhagen, Denmark
- 13 Departamento de Física, Universidad de Oviedo, Avda. Calvo Sotelo s/n, Oviedo, Spain
- 14 Department of Astronomy and Astrophysics, University of Toronto, 50 Saint George Street, Toronto, Ontario, Canada

- ¹⁵ Department of Physics & Astronomy, University of British Columbia, 6224 Agricultural Road, Vancouver, British Columbia, Canada
- ¹⁶ Department of Physics and Astronomy, University of Southern California, Los Angeles, California, U.S.A.
- ¹⁷ Department of Physics, Gustaf Hällströmin katu 2a, University of Helsinki, Helsinki, Finland
- ¹⁸ Department of Physics, Purdue University, 525 Northwestern Avenue, West Lafayette, Indiana, U.S.A.
- ¹⁹ Department of Physics, University of California, Berkeley, California, U.S.A.
- ²⁰ Department of Physics, University of California, One Shields Avenue, Davis, California, U.S.A.
- ²¹ Department of Physics, University of California, Santa Barbara, California, U.S.A.
- ²² Department of Physics, University of Illinois at Urbana-Champaign, 1110 West Green Street, Urbana, Illinois, U.S.A.
- ²³ Dipartimento di Fisica G. Galilei, Università degli Studi di Padova, via Marzolo 8, 35131 Padova, Italy
- ²⁴ Dipartimento di Fisica, Università La Sapienza, P. le A. Moro 2, Roma, Italy
- ²⁵ Dipartimento di Fisica, Università degli Studi di Milano, Via Celoria, 16, Milano, Italy
- ²⁶ Dipartimento di Fisica, Università degli Studi di Trieste, via A. Valerio 2, Trieste, Italy
- ²⁷ Dipartimento di Fisica, Università di Ferrara, Via Saragat 1, 44122 Ferrara, Italy
- ²⁸ Dipartimento di Fisica, Università di Roma Tor Vergata, Via della Ricerca Scientifica, 1, Roma, Italy
- ²⁹ Discovery Center, Niels Bohr Institute, Blegdamsvej 17, Copenhagen, Denmark
- ³⁰ Dpto. Astrofísica, Universidad de La Laguna (ULL), E-38206 La Laguna, Tenerife, Spain
- ³¹ European Southern Observatory, ESO Vitacura, Alonso de Cordova 3107, Vitacura, Casilla 19001, Santiago, Chile
- ³² European Space Agency, ESAC, Planck Science Office, Camino bajo del Castillo, s/n, Urbanización Villafranca del Castillo, Villanueva de la Cañada, Madrid, Spain
- ³³ European Space Agency, ESTEC, Keplerlaan 1, 2201 AZ Noordwijk, The Netherlands
- ³⁴ Finnish Centre for Astronomy with ESO (FINCA), University of Turku, Väisäläntie 20, FIN-21500, Piikkiö, Finland
- ³⁵ Haverford College Astronomy Department, 370 Lancaster Avenue, Haverford, Pennsylvania, U.S.A.
- ³⁶ Helsinki Institute of Physics, Gustaf Hällströmin katu 2, University of Helsinki, Helsinki, Finland
- ³⁷ INAF - Osservatorio Astrofisico di Catania, Via S. Sofia 78, Catania, Italy
- ³⁸ INAF - Osservatorio Astronomico di Padova, Vicolo dell'Osservatorio 5, Padova, Italy
- ³⁹ INAF - Osservatorio Astronomico di Roma, via di Frascati 33, Monte Porzio Catone, Italy
- ⁴⁰ INAF - Osservatorio Astronomico di Trieste, Via G.B. Tiepolo 11, Trieste, Italy
- ⁴¹ INAF/IASF Bologna, Via Gobetti 101, Bologna, Italy
- ⁴² INAF/IASF Milano, Via E. Bassini 15, Milano, Italy
- ⁴³ INRIA, Laboratoire de Recherche en Informatique, Université Paris-Sud 11, Bâtiment 490, 91405 Orsay Cedex, France
- ⁴⁴ IPAG: Institut de Planétologie et d'Astrophysique de Grenoble, Université Joseph Fourier, Grenoble 1 / CNRS-INSU, UMR 5274, Grenoble, F-38041, France
- ⁴⁵ ISDC Data Centre for Astrophysics, University of Geneva, ch. d'Ecogia 16, Versoix, Switzerland
- ⁴⁶ Imperial College London, Astrophysics group, Blackett Laboratory, Prince Consort Road, London, SW7 2AZ, U.K.
- ⁴⁷ Infrared Processing and Analysis Center, California Institute of Technology, Pasadena, CA 91125, U.S.A.
- ⁴⁸ Institut Néel, CNRS, Université Joseph Fourier Grenoble I, 25 rue des Martyrs, Grenoble, France
- ⁴⁹ Institut d'Astrophysique Spatiale, CNRS (UMR8617) Université Paris-Sud 11, Bâtiment 121, Orsay, France
- ⁵⁰ Institut d'Astrophysique de Paris, CNRS UMR7095, Université Pierre & Marie Curie, 98 bis boulevard Arago, Paris, France
- ⁵¹ Institut de Radioastronomie Millimétrique (IRAM), Avenida Divina Pastora 7, Local 20, 18012 Granada, Spain
- ⁵² Institute of Astronomy and Astrophysics, Academia Sinica, Taipei, Taiwan
- ⁵³ Institute of Astronomy, University of Cambridge, Madingley Road, Cambridge CB3 0HA, U.K.
- ⁵⁴ Institute of Theoretical Astrophysics, University of Oslo, Blindern, Oslo, Norway
- ⁵⁵ Instituto de Astrofísica de Canarias, C/Vía Láctea s/n, La Laguna, Tenerife, Spain
- ⁵⁶ Instituto de Física de Cantabria (CSIC-Universidad de Cantabria), Avda. de los Castros s/n, Santander, Spain
- ⁵⁷ Istituto di Fisica del Plasma, CNR-ENEA-EURATOM Association, Via R. Cozzi 53, Milano, Italy
- ⁵⁸ Jet Propulsion Laboratory, California Institute of Technology, 4800 Oak Grove Drive, Pasadena, California, U.S.A.
- ⁵⁹ Jodrell Bank Centre for Astrophysics, Alan Turing Building, School of Physics and Astronomy, The University of Manchester, Oxford Road, Manchester, M13 9PL, U.K.
- ⁶⁰ Kavli Institute for Cosmology Cambridge, Madingley Road, Cambridge, CB3 0HA, U.K.
- ⁶¹ LERMA, CNRS, Observatoire de Paris, 61 Avenue de l'Observatoire, Paris, France
- ⁶² Laboratoire AIM, IRFU/Service d'Astrophysique - CEA/DSM - CNRS - Université Paris Diderot, Bât. 709, CEA-Saclay, F-91191 Gif-sur-Yvette Cedex, France
- ⁶³ Laboratoire Traitement et Communication de l'Information, CNRS (UMR 5141) and Télécom ParisTech, 46 rue Barrault F-75634 Paris Cedex 13, France
- ⁶⁴ Laboratoire de Physique Subatomique et de Cosmologie, CNRS/IN2P3, Université Joseph Fourier Grenoble I, Institut National Polytechnique de Grenoble, 53 rue des Martyrs, 38026 Grenoble cedex, France
- ⁶⁵ Laboratoire de l'Accélérateur Linéaire, Université Paris-Sud 11, CNRS/IN2P3, Orsay, France
- ⁶⁶ Lawrence Berkeley National Laboratory, Berkeley, California, U.S.A.
- ⁶⁷ Max-Planck-Institut für Astrophysik, Karl-Schwarzschild-Str. 1, 85741 Garching, Germany
- ⁶⁸ Max-Planck-Institut für Radioastronomie, Auf dem Hügel 69, 53121 Bonn, Germany
- ⁶⁹ MilliLab, VTT Technical Research Centre of Finland, Tietotie 3, Espoo, Finland
- ⁷⁰ National University of Ireland, Department of Experimental Physics, Maynooth, Co. Kildare, Ireland
- ⁷¹ Niels Bohr Institute, Blegdamsvej 17, Copenhagen, Denmark
- ⁷² Observational Cosmology, Mail Stop 367-17, California Institute of Technology, Pasadena, CA, 91125, U.S.A.
- ⁷³ SISSA, Astrophysics Sector, via Bonomea 265, 34136, Trieste, Italy
- ⁷⁴ SUPA, Institute for Astronomy, University of Edinburgh, Royal Observatory, Blackford Hill, Edinburgh EH9 3HJ, U.K.
- ⁷⁵ School of Physics and Astronomy, Cardiff University, Queens Buildings, The Parade, Cardiff, CF24 3AA, U.K.
- ⁷⁶ Space Sciences Laboratory, University of California, Berkeley, California, U.S.A.
- ⁷⁷ Special Astrophysical Observatory, Russian Academy of Sciences, Nizhnij Arkhiz, Zelenchukskiy region, Karachai-Cherkessian Republic, 369167, Russia
- ⁷⁸ Stanford University, Dept of Physics, Varian Physics Bldg, 382 Via Pueblo Mall, Stanford, California, U.S.A.
- ⁷⁹ Université de Toulouse, UPS-OMP, IRAP, F-31028 Toulouse cedex 4, France
- ⁸⁰ Universities Space Research Association, Stratospheric Observatory for Infrared Astronomy, MS 211-3, Moffett Field, CA 94035, U.S.A.

- ⁸¹ University of Granada, Departamento de Física Teórica y del Cosmos, Facultad de Ciencias, Granada, Spain
- ⁸² University of Miami, Knight Physics Building, 1320 Campo Sano Dr., Coral Gables, Florida, U.S.A.
- ⁸³ Warsaw University Observatory, Aleje Ujazdowskie 4, 00-478 Warszawa, Poland